AD-A119 869 NAVAL RESEARCH LAB WASHINGTON DC F/G 20/7
EQUILIBRIUM OF A HIGH CURRENT ELECTRON RING IN A MODIFIED BETAT--ETC(U)
SEP 82 C A KAPETANAKOS, P SPRANGLE
UNCLASSIFIED NRL-MR-4905 NL

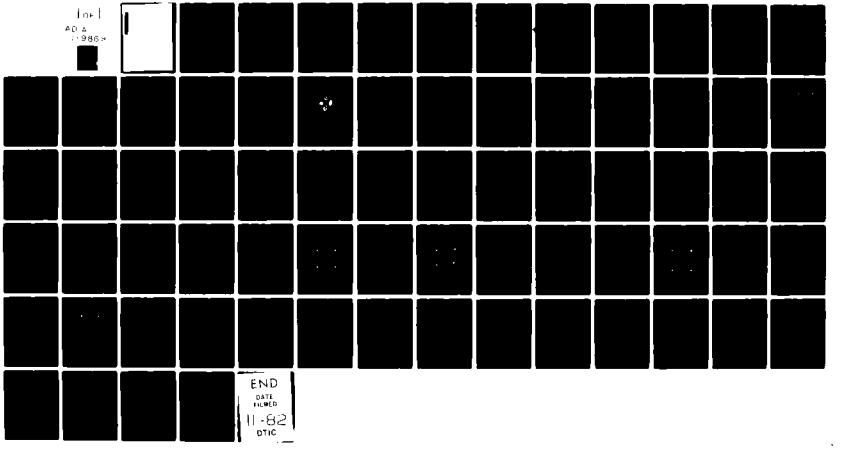

END
DATE FILMED
11-82
DTIC

SECURITY CLASSIFICATION OF THIS PAGE (When Data Entered)

REPORT DOCUMENTATION PAGE	READ INSTRUCTIONS BEFORE COMPLETING FORM
1. REPORT NUMBER: NRL Memorandum Report 4905	2. GOVT ACCESSION NO.: AD-A129869
3. RECIPIENT'S CATALOG NUMBER	
4. TITLE (and Subtitle): EQUILIBRIUM OF A HIGH CURRENT ELECTRON RING IN A MODIFIED BETATRON ACCELERATOR	5. TYPE OF REPORT & PERIOD COVERED: Interim report on a continuing NRL problem.
	6. PERFORMING ORG. REPORT NUMBER
7. AUTHOR(s): C.A. Kapetanakos, P. Sprangle, D.P. Chernin*, S.J. Marsh**, and I. Haber	8. CONTRACT OR GRANT NUMBER(s)
9. PERFORMING ORGANIZATION NAME AND ADDRESS: Naval Research Laboratory, Washington, DC 20375	10. PROGRAM ELEMENT, PROJECT, TASK AREA & WORK UNIT NUMBERS: 61153N; RR011-09-4E; 47-0924-0-2
11. CONTROLLING OFFICE NAME AND ADDRESS: Office of Naval Research, Arlington, VA 22217	12. REPORT DATE: September 30, 1982
	13. NUMBER OF PAGES: 71
14. MONITORING AGENCY NAME & ADDRESS(if different from Controlling Office)	15. SECURITY CLASS. (of this report): UNCLASSIFIED
	15a. DECLASSIFICATION/DOWNGRADING SCHEDULE

16. DISTRIBUTION STATEMENT (of this Report)

Approved for public release; distribution unlimited.

17. DISTRIBUTION STATEMENT (of the abstract entered in Block 20, if different from Report)

18. SUPPLEMENTARY NOTES

*Present address: Berkeley Research Associates, Springfield, VA 22150
**Present address: Sachs/Freeman Associates, Bladensburg, MD 20710

19. KEY WORDS (Continue on reverse side if necessary and identify by block number)

Modified betatron
High energy accelerators
Beam equilibrium

20. ABSTRACT (Continue on reverse side if necessary and identify by block number)

This paper addresses the dynamics of an ultra-high current electron ring in a modified betatron configuration. Our studies include analytical and numerical results for both "cold" and "hot" rings. It has been found that the walls surrounding the ring and toroidal effects (hoop stresses) play a very important role in the dynamics of the ring, even when the wall conductivity is infinite. For finite wall conductivity, the diffusion of

(Continues)

DD FORM 1 JAN 73 1473 EDITION OF 1 NOV 65 IS OBSOLETE
S/N 0102-014-6601

SECURITY CLASSIFICATION OF THIS PAGE (When Data Entered)

20. ABSTRACT (Continued)

the ring's self magnetic field profoundly impacts its dynamics and in general the equilibrium could be lost if means are not provided to compensate for this effect. In addition, it has been found that the Grad B drift is not important, except when the bounce frequency is very small.

The general conclusion of these studies is that equilibrium states of ultra-high current rings in a modified betatron configuration exist over a wide range of parameters. These states are accessible and within the realm of existing pulsed power technology.

CONTENTS

I. INTRODUCTION 1

II. ORBIT STABILITY OF A COLD RING WITHOUT SURROUNDING WALLS AND TOROIDAL CORRECTIONS 3

III. WALL EFFECTS ON THE MACROSCOPIC MOTION OF A COLD BEAM 7

a. Without Toroidal Corrections 7
b. With Toroidal Corrections 16

IV. ACCELERATION 23

V. GRAD B DRIFT IN THE MODIFIED BETATRON 36

VI. THE EFFECT OF EMITTANCE 43

VII. SUMMARY 54

ACKNOWLEDGMENTS 54

APPENDIX A 55

APPENDIX B 62

REFERENCES 67

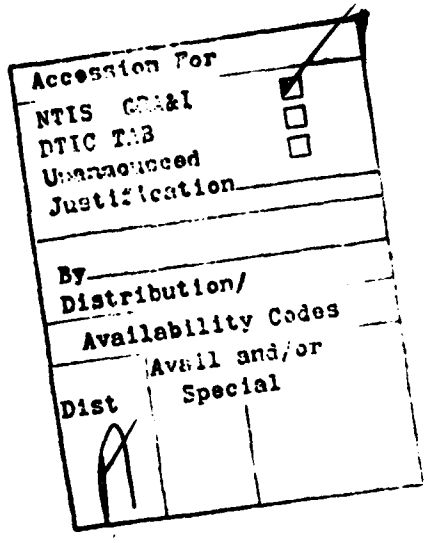

EQUILIBRIUM OF A HIGH CURRENT ELECTRON RING IN A MODIFIED BETATRON ACCELERATOR

I. Introduction

Over the last few years, several laboratories[1-7] have been engaged in studies that are aimed to assess the feasibility of developing ultra high current accelerators. These studies are mainly motivated by the potential application of high energy, high current electron beams in nuclear physics research, medical radiography and the fusion program.

In general, the effort is not directed toward developing novel accelerating schemes but rather in modifying or improving the existing accelerator technology. Among the various proposed modifications, the addition of a strong toroidal magnetic field to a conventional betatron[8,9] has attracted considerable attention[4-7] and the configuration has been named the modified betatron.

In this paper we analyze and discuss the dynamics of a high current electron ring confined in a modified betatron configuration. When the intense electron ring is surrounded by a finite conductivity wall, its dynamics can be divided, rather naturally, into three distinct phases: The pre-acceleration phase follows the injection and trapping of the electron beam. The duration of this phase is short, typically a few μsec and the conducting wall surrounding the ring can be treated as perfect conductor. The pre-acceleration phase is followed by the diffusion phase, which lasts for a time that is of the order of the magnetic field diffusion time. During the diffusion phase the self magnetic field of the beam diffuses out of the metal torus. As a result the electron energy is reduced and the hoop stresses increase, but at different rates. Therefore, the equilibrium will be lost if means are not provided to balance these two effects. The last phase, i.e., the main acceleration, starts after the self magnetic field diffuses out of the torus and has a duration that is comparable with the acceleration time. For most of the third

Manuscript submitted August 17, 1982.

phase the energy of the ring has increased substantially and thus the effect of the self fields is appreciably diminished.

The present work addresses the dynamics of high current ring in a modified betatron configuration. It includes both analytical and computational studies for "cold" as well as "hot" electron rings. The main conclusions are: First, if the energy of the injected electrons is not exactly equal to the energy corresponding to the equilibrium orbit, which is assumed to coincide with the minor axis of the torus, the center of the orbit is displaced from the center of the minor cross-section of the torus. The displacement is proportional to the energy mismatch. This imposes very stringent constraints on the injector. Second, during the diffusion of the self magnetic field of the ring out of the chamber, the equilibrium can be lost if means are not provided to balance the change of the ring equilibrium radius that are due to the reduction of the relativistic factor γ_o and the increase of hoop stresses. Third, the modification in the flux rule for high current rings can be ignored, provided that ν/γ_o^3 (ν = Budker parameter) is very small. Fourth, with the exception of the expansion of the minor cross-section of the ring, finite emittance does not have any other noticable effect on the equilibrium, and fifth, considerably higher axial energy spread can be tolerated in high than in low current rings.

The general and most important conclusion of these studies is that equilibrium states of high current rings in a modified betatron configuration exist over a wide range of parameters. These equilibria are realistic and accessible with existing technology.

II. Orbit Stability of a Cold Ring Without Surrounding Walls and Toroidal Corrections

The stability of a single particle orbit, when thermal effects, wall effects and toroidal corrections are neglected, has been considered previously.[4] Using the coordinate system shown in Fig. 1 and assuming that the external field components vary as

$$B_z(r,t) \cong B_{oz}(t)\ \{1 - n\ (r - r_o)/r_o\}, \tag{1a}$$

$$B_r(r,t) \cong - B_{oz}(t)\ nz/r_o, \tag{1b}$$

$$E_\theta\ (r,t) = - \frac{1}{rc} \int_o^r r'dr'\ \frac{\partial B_z}{\partial t}\ (r',\ t), \tag{1c}$$

and

$$B_\theta(r) \cong B_{o\theta}\ \{1 - (r - r_o)/r_o\}, \tag{1d}$$

it has been determined that for $B_\theta >> B_z$ and $\nu/\gamma_o << 1$ the orbits are stable, provided that the following condition is satisfied

$$n_s \leq (B_{o\theta}/2B_{oz})^2. \tag{2}$$

In the above equations $B_z(r,t)$ is the axial and $B_r(r,t)$ is the radial component of the betatron field, $B_\theta(r)$ is the toroidal magnetic field, $E_\theta(r,t)$ is the induced

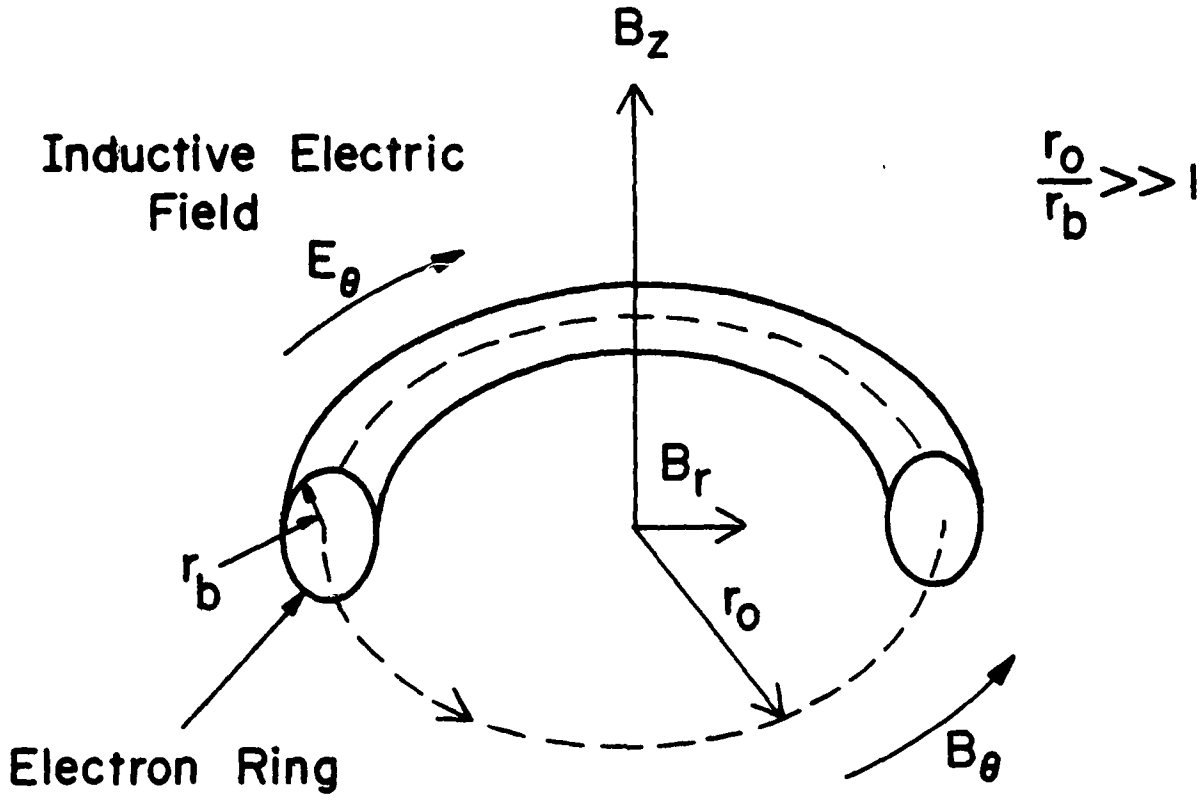

Figure 1. Schematic of the modified betatron configuration and system of coordinates used in the analysis.

electric field, n is the external field index, r_o, z_o are the coordinates of the center of the electron ring and n_s is the self-field index. The self-field index is defined as

$$n_s = \omega_b^2/(2\gamma_o\Omega_{oz}^2) = 2(\nu/\gamma_o)\ (c/\Omega_{oz}r_b)^2, \qquad (3)$$

where $\omega_b^2 \{= 4\pi e^2 n_o/m\}$ is the beam plasma frequency squared, γ_o is the relativistic factor, Ω_{oz} $\{=eB_{oz}/mc\}$ is the cyclotron frequency corresponding to the axial component of the betatron field, r_b is the minor radius of the beam and ν is Budker's parameter, i.e., the product of the number of electrons per unit length times the electron classical radius.

The electron beam current that can be stably confined in a modified betatron can be obtained by substituting Eq. (3) into Eq. (2) and is

$$I_{mb} \leq 2.1\ (r_b/r_o)^2\ \gamma_o^3\beta_o^3\ (B_{o\theta}/B_{oz})^2\ \{KA\}. \qquad (4)$$

where $\beta_o = v_o/c$. When $\gamma_o >> 1$, then $r_o\Omega_{oz}/\gamma_o = c$ and Eq. (4) becomes

$I_{mb} \leq 7.22 \times 10^{-7}\ r_b^2\gamma_o B_{o\theta}^2\ \{KA\}$, with r_b in cm and $B_{o\theta}$ in Gauss.

In addition, it has been shown under the same conditions but with $B_\theta = 0$ (conventional betatron), the beam is stable provided

$$n_s < 1/2, \text{ conventional betatron.} \quad (B_\theta = 0) \qquad (5)$$

The electron beam current that can be stably confined in a conventional betatron can be obtained by substituting Eq. (3) into Eq. (5) and is

$$I_{cb} \leq 4.2\ (r_b/r_o)^2 \gamma_o^3 \beta_o^3\ \{KA\}. \tag{6}$$

or

$$I_{cb} \leq 14.44 \times 10^{-7}\ r_b^2 \gamma_o B_{oz}^2\ \{KA\},$$

when $\gamma_o \gg 1$. The ratio of I_{mb} to I_{cb} obtained from Eqs. (4) and (6) is

$$\frac{I_{mb}}{I_{cb}} = 1/2\ (B_{o\theta}/B_{oz})^2.$$

The above relation indicates that for $B_{o\theta} \gg B_{oz}$, the electron beam current that can be stably confined in a modified betatron substantially exceeds the current that can be confined in a conventional betatron.

The modified betatron stability condition given in Eq. (2) can be easily obtained from the well known confined equilibrium condition[10]

$$2(\omega_b^2/\Omega_c^2) \leq 1, \text{ (non-relativistic)} \tag{7}$$

where ω_b is the beam plasma frequency and Ω_c is the cyclotron frequency. For relativistic energies and taking into account the self magnetic field of the beam ω_b^2 becomes

$$\omega_b^2 = \left(\frac{\omega_b^2}{\gamma_o}\right) \underbrace{\frac{1}{\gamma_o^2}}_{\text{self field correction}}, \tag{8}$$

and

$$\Omega_c^2 + \Omega_\theta^2/\gamma_o^2. \tag{9}$$

Substituting Eqs. (8) and (9) into Eq. (7) we obtain the stability condition of Eq. (2). The equality sign in Eq. (2) gives the maximum electron density that can be supported at a specific value of $B_{o\theta}/B_{oz}$ and the corresponding equilibrium is known as Brillouin flow.[10]

III. Wall Effects on the Macroscopic Motion of a Cold Beam

In this section we analyze the effects of surrounding walls on the motion of the center of the beam. In the first sub-section, it is assumed that the perfect conductor that surrounds the beam is a straight cylindrical pipe of circular cross-section and thus toroidal effects (hoop stresses) are omitted. These effects are included in the second sub-section.

a. Without toroidal corrections

Consider a pencil-like electron beam inside a straight, perfectly conducting cylindrical pipe of circular cross-section as shown in Fig. 2. The center of the beam is located at a distance Δr, Δz from the center of the minor cross-section of the pipe. As a result of the induced charges on the wall, the center of the beam will experience a radial, outward directed force, which for small displacements, i.e., Δr, $\Delta z \ll a$ is given by

$$\vec{F}_E = 2\pi e^2 n_o (r_b/a)^2 \{\Delta r \hat{e}_r + \Delta z \hat{e}_z\}, \tag{10}$$

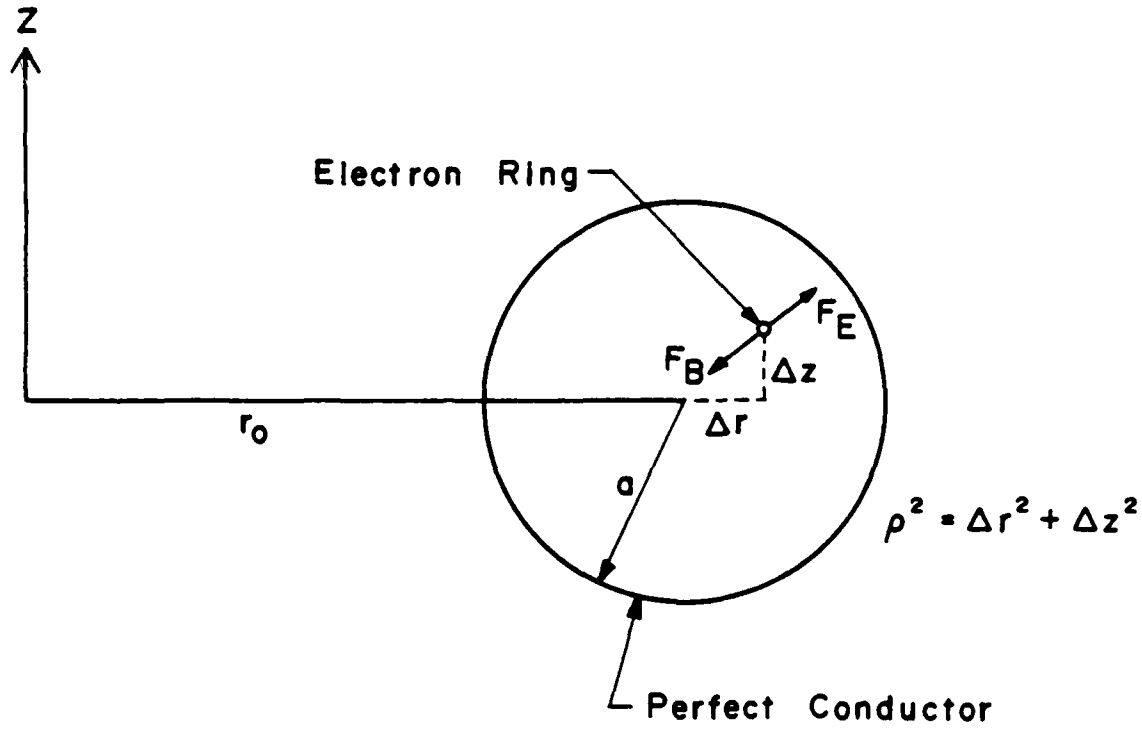

Figure 2. Wall (images) forces acting on a pencil-like electron beam, situated inside a perfectly conducting cylindrical pipe.

where a is the cylinder radius and n_o the uniform beam density.

Similarly, as a result of the induced current on the wall, the center of the beam will experience a radial force that is directed toward the opposite direction than F_E and is given by

$$\vec{F}_B = - \beta_o^2 \vec{F}_E. \tag{11}$$

Using the external fields of Eq. (1) and the induced fields of Eqs. (10) and (11), the equations describing the temporal linear evolution of the beam's center, for time independent applied fields, are:

$$\Delta\ddot{r} + \tilde{\omega}_r^2 \Delta r = \frac{\Omega_{o\theta}}{\gamma_o} \Delta\dot{z} + \left(\frac{\Omega_{oz}}{\gamma_o}\right) \frac{\langle \delta P_\theta \rangle}{\gamma_o m r_o} \tag{12}$$

and

$$\Delta\ddot{z} + \tilde{\omega}_z^2 \Delta z = - \frac{\Omega_{o\theta}}{\gamma_o} \Delta\dot{r}, \tag{13}$$

where $\tilde{\omega}_r^2 = (\Omega_{oz}/\gamma_o)^2(1 - n - n_s \frac{r_b^2}{a^2})$, $\tilde{\omega}_z^2 = (\Omega_{oz}/\gamma_o)^2(n - n_s \frac{r_b^2}{a^2})$,

$\Omega_{o\theta} = eB_{o\theta}/mc$, $\Omega_{oz} = eB_{oz}/mc$, $\frac{\delta\gamma_o}{\gamma_o} = \frac{\beta_o \langle \delta P_\theta \rangle}{\gamma_o m r_o c}$ and δP_θ is the difference between the canonical angular momentum of an electron at (r,z) and its corresponding value at the equilibrium orbit (r_o,o). The average is over initial coordinates and velocities. Equations (12) and (13) do not include the self electric and self magnetic fields, because both these fields are zero at the center of a straight

beam. In addition, the non-linear terms $\frac{\Delta r}{r_o}\frac{\Omega_{o\theta}}{\gamma_o}\dot{\Delta z}$ and $\frac{\Delta r}{r_o}\frac{\Omega_{o\theta}}{\gamma_o}\dot{\Delta r}$ have been omitted from Eqs. (12) and (13). These two terms have their origin in the gradient of the toroidal magnetic field and are considered in Section V. In general these terms are not significant except in the limit $\tilde{\omega}_r \to o$.

In Eq. (12), $\delta\gamma_o = \beta_o\langle\delta P_\theta\rangle/mr_oc$ indicates the energy mismatch, i.e., the difference between the energy of the reference electron (moving along the axis of the beam) and the energy required for the same electron to move on the equilibrium orbit (r_o,o). The solution of Eqs. (12) and (13), for time independent fields, is

$$\Delta r = \frac{\Omega_{oz}\langle\delta P_\theta\rangle}{\gamma_o^2\tilde{\omega}_r^2 r_o m} + \sum_{j=1}^{4} c_j\,(\tilde{\omega}_z^2 - \omega_j^2)^{1/2}\; e^{i\omega_j t}, \tag{14}$$

and

$$\Delta z = \sum_{j=1}^{4} c_j\,(\omega_j^2 - \tilde{\omega}_r^2)^{1/2}\; e^{i\omega_j t}, \tag{15}$$

where c_j is a constant and

$$\omega_j^2 = 1/2\,\{\tilde{\omega}_r^2 + \tilde{\omega}_z^2 + (\Omega_{o\theta}/\gamma_o)^2 \pm [(\tilde{\omega}_r^2 + \tilde{\omega}_z^2 + (\Omega_{o\theta}/\gamma_o)^2)^2 - 4\tilde{\omega}_r^2\,\tilde{\omega}_z^2\,]^{1/2}\}. \tag{16}$$

The first term on the RHS of Eq. (14) gives the displacement of the center of the orbit from the center of the surrounding cylindrical pipe and can be written as

$$\Delta r_o = \frac{\langle\delta P_\theta\rangle/\gamma_o}{(\Omega_{oz}/\gamma_o)\,(1 - n - n_s r_b^2/a^2)mr_o} \tag{17}$$

Equation (16) has four roots. Two of them are fast (plus sign) and two are slow (minus sign). When $B_\theta >> B_z$, the slow mode becomes

$$\omega_j^2 = \omega_B^2 = \left(\frac{\tilde{\omega}_r \tilde{\omega}_z}{\Omega_{o\theta}/\gamma_o}\right)^2 = \left(\frac{B_{oz}}{B_{o\theta}}\right)^2 \left(\frac{\Omega_{oz}}{\gamma_o}\right)^2 \left(1 - n - n_s \frac{r_b^2}{a^2}\right)\left(n - n_s \frac{r_b^2}{a^2}\right), \qquad (18)$$

and the fast mode is $= (\Omega_{o\theta}/\gamma_o)$. Equation (18) is plotted in Fig. 3 for two values of external field index. For $n > 1/2$, ω_B^2 is negative when $1 - n < \frac{n_s r_b^2}{a^2} < n$ and for $n < 1/2$, ω_B^2 is negative when $n < \frac{n_s r_b^2}{a^2} < 1 - n$. Negative values of ω_B^2 indicate that the beam motion is unstable and the orbit in the r,z plane is open. Since the parameter $n_s r_b^2/a^2$ scales as γ_o^{-3}, during acceleration $n_s r_b^2/a^2$ decreases rapidly. Therefore, in order to avoid the instability, it is necessary that before the commencement of the acceleration the parameter $n_s r_b^2/a^2$ is less than $1 - n$ when $n > 1/2$ and less than n when $n < 1/2$. This implies that the injected beam current should be limited to

$$I \leq 8.5\ (1 - n)\ \beta_o \gamma_o^3 a^2/r_o^2\ \{KA\} \text{ for } n > 1/2$$

and

$$I \leq 8.5\ n\beta_o \gamma_o^3 a^2/r_o^2\ \{KA\} \text{ for } n < 1/2.$$

It is apparent that these two constraints are rather lenient.

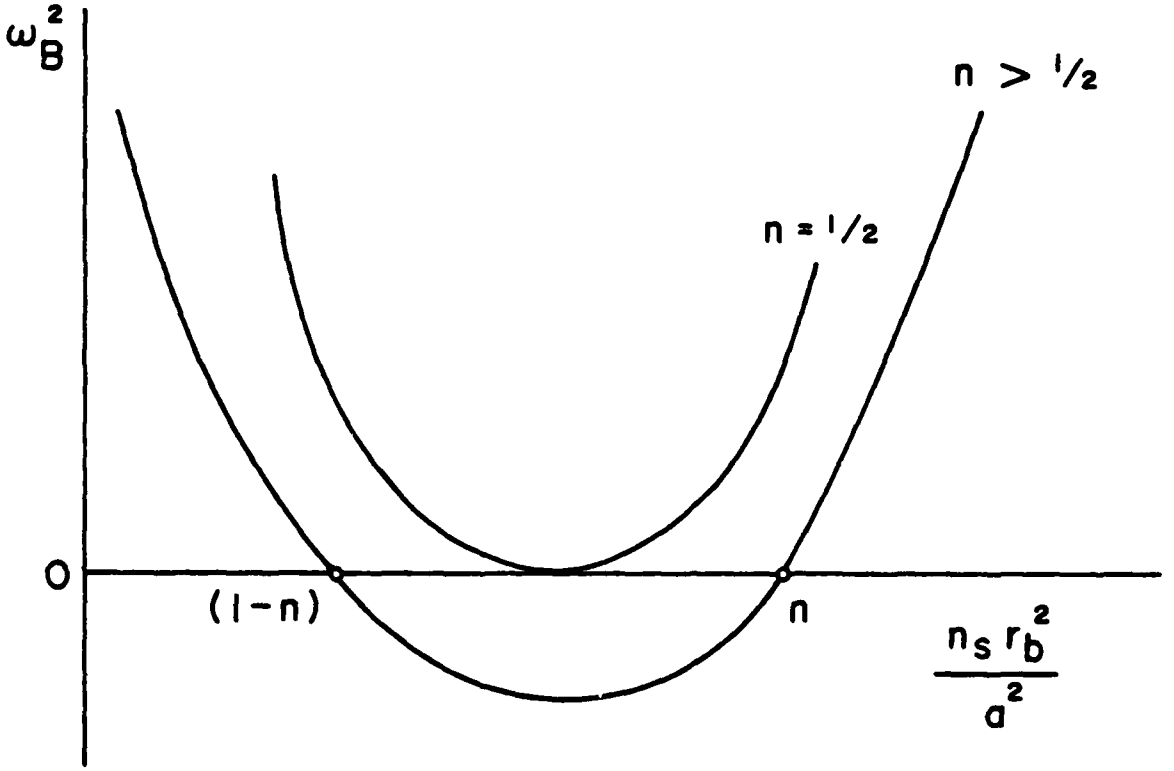

Figure 3. Bounce frequency-squaredas a function of $n_s r_b^2/a^2$, with the field index n as a parameter. The orbits are open when $\omega_B^2 < 0$ and closed when $\omega_B^2 > 0$.

The orbit of the ring's center is described by

$$\Delta r(t) = [\Delta r(o) - \Delta r_o] \cos \omega_B t + \frac{\Delta \dot{r}(o)}{\omega_B} \sin \omega_B t + \Delta r_o,$$

$$\Delta z(t) = \Delta r(o) \cos (\omega_B t) + \frac{\Delta \dot{z}(o)}{\omega_B} \sin (\omega_B t),$$

where the initial velocities and displacements are related by

$$\Delta \dot{r}(o) = - [\tilde{\omega}_z^2/(\Omega_{o\theta}/\gamma_o)] \Delta z(o),$$

$$\Delta \dot{z}(o) = [\tilde{\omega}_r^2/(\Omega_{o\theta}/\gamma_o)] \Delta r(o) + (\frac{\Omega_{oz}}{\Omega_{o\theta}}) \frac{\langle \delta P_\theta \rangle}{\gamma_o m r_o},$$

and

$$\langle \delta P_\theta \rangle = \gamma_o m r_o (v_\theta - r_o \Omega_{oz}/\gamma_o).$$

The predictions of Eq. (18) are in good agreement with the results of computer simulation shown in Fig. 4. This figure shows four snap-shots of the beam in the r,z plane. At t = 0 the circular electron beam is injected near the center of the pipe. The values of the various parameters are listed in Table I. The electron beam current is kept low (1 KA) in order to minimize the toroidal effects. As can be seen from Fig. 4, the center of the electron beam describes a circle in the r,z plane with a period of about 188 nsec. For the same parameters Eq. (18) predicts a period $\tau_B = 2\pi/\omega_B \tilde{=} 180$ nsec. These numerical results are discussed further in the next sub-section.

The displacement of the orbit's center because of the energy mismatch [Eq. (17)], imposes very stringent constraints on the injector. This becomes apparent when we consider some limiting cases. For example, when n = ½ and $n_s r_b^2 \ll 1$, Eq. (17) is reduced to

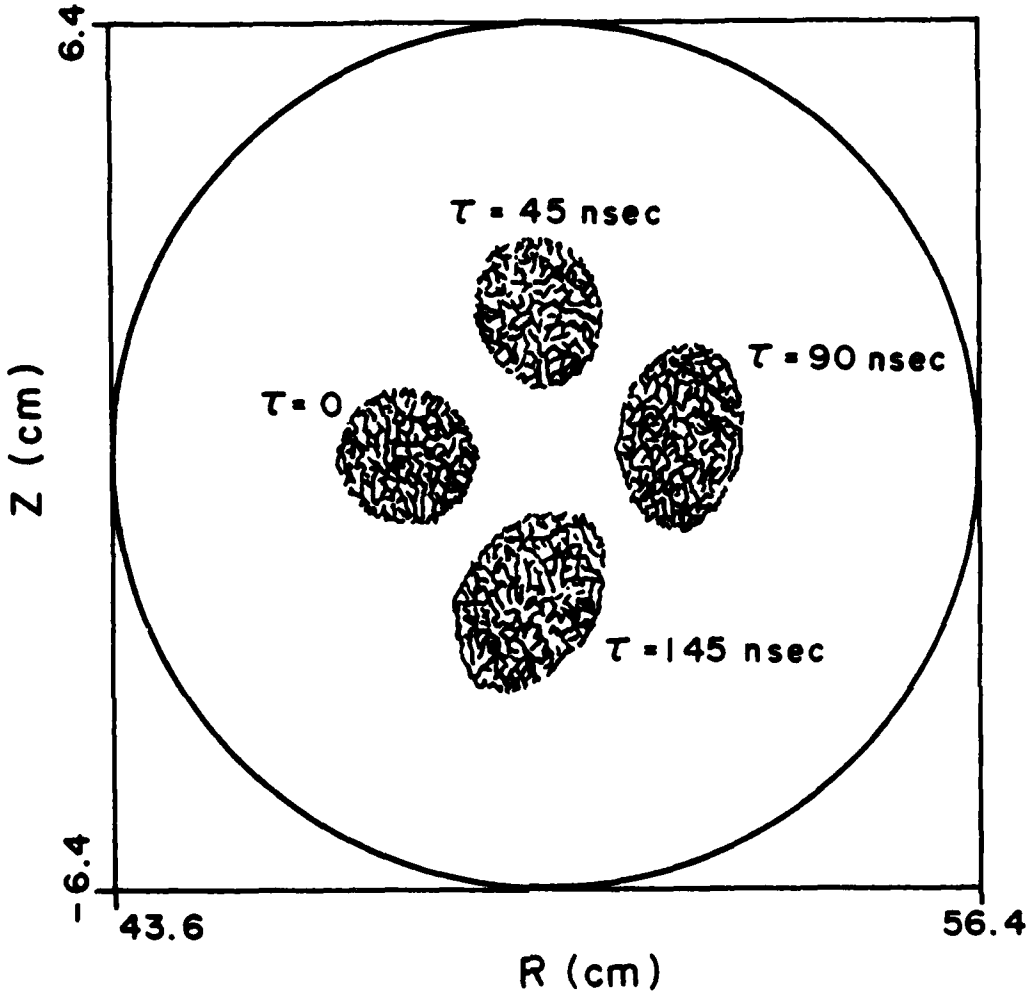

Figure 4. Snap-shots of the electron ring minor cross-section at four different times. The values of the various parameters are listed in Table I. The center of the ring's minor cross-section describes a circle.

Table I.

Parameters	
Beam Energy (MeV)	3
Beam Current (kA)	1
Beam Minor Radius (cm)	1
Beam Major Radius (cm)	50
Torus minor radius (cm)	6.4
Vertical magnetic field (G)	240
Toroidal magnetic field (kG)	2
External field index	0.47
Self field index	0.88

$$\frac{\Delta r_o}{r_o} \approx 2(\delta\gamma_o/\gamma_o). \qquad (19)$$

Equation (19) predicts that for a major radius $r_o = 100$ cm, the ratio $\delta\gamma_o/\gamma_o$ should be less than 1% in order the displacement of the orbit to be less than 2 cm. The condition $\delta\gamma_o/\gamma_o \leq 1\%$ requires that the uncertainty in energy should be less than 35 KeV, when the energy of the injected beam is 3 MeV. Although such a small energy uncertainty can be attained with sophisticated injectors, there are other factors, such as space charge and inductive effects, which contribute substantially to the uncertainty of energy. Although the displacement cannot be eliminated, its negative impact can be alleviated by elongating the minor cross-section of the torus along the r-direction.

b. Toroidal Corrections[5,11]

The cause of these effects is the finite curvature of the electron beam orbit. For relative large aspect ratio $r_o/r_b \gg 1$ beams, the toroidal effects become important when ν/γ_o exceeds a few percent. Previous work[12] on toroidal effects was limited to "bare" rings, i.e., without surrounding conducting walls. In this sub-section we briefly analyze the toroidal corrections for the more realistic geometry shown in Fig. 5, i.e., including the effect of conducting wall around the beam. Since different physics issues are involved in the case of a "bare" and "shielded" rings, it is appropriate to start our discussion with a bare ring.

Consider on intense electron ring as shown in Fig. 5, but without the toroidal chamber. At the inner edge of the RHS cross-section of the ring the self-magnetic field is greater than that of a straight beam with the same parameters, because of the contribution from the LHS of the ring. At the outer edge of the cross-section, the self magnetic field is reduced because the contribution from the LHS of the ring

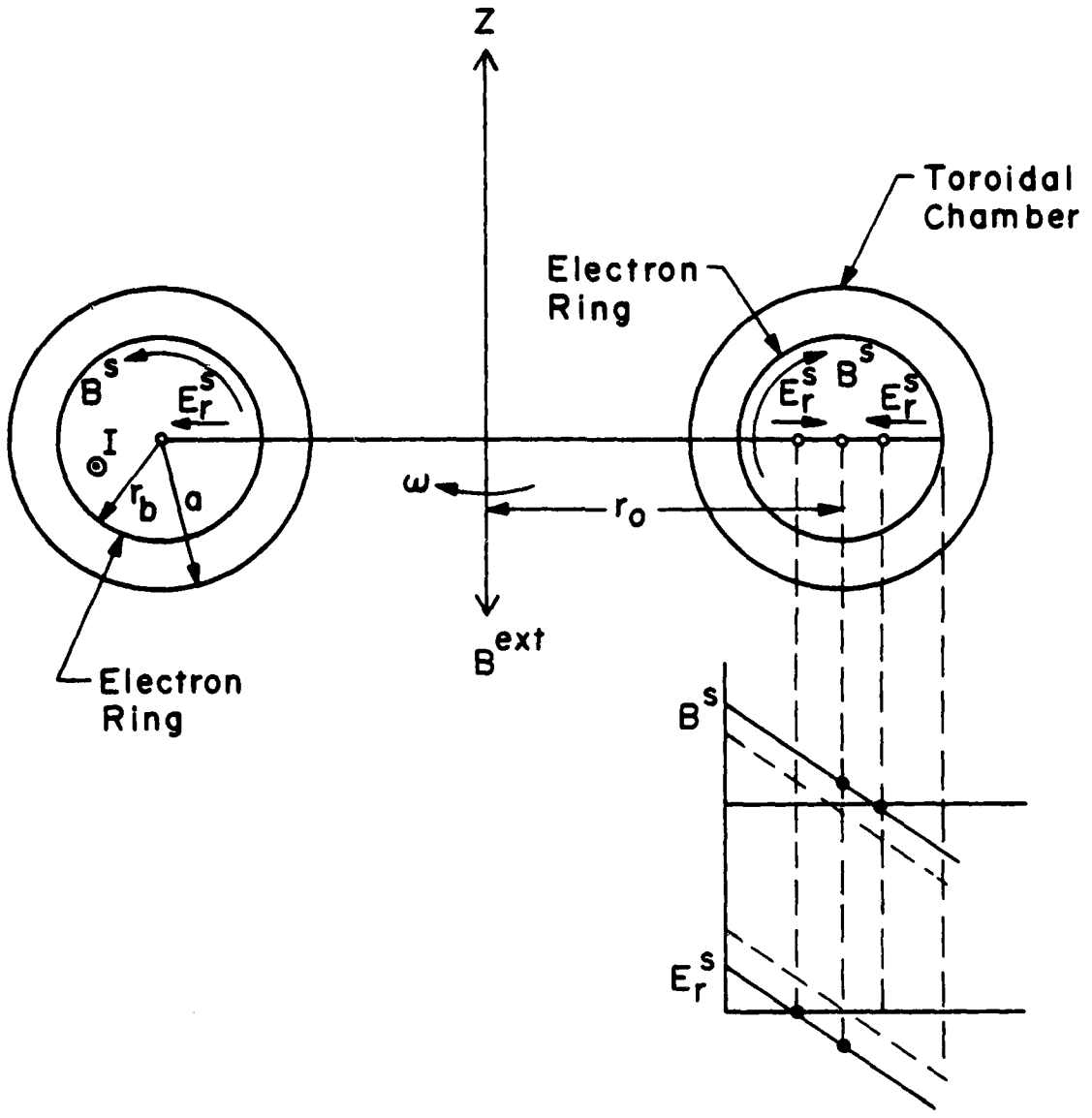

Figure 5. An electron ring inside a conducting toroidal chamber. Because of the toroidal effects, neither the self-electric not the self magnetic field is zero at the geometric center of the ring.

has opposite polarity than the local field. Thus, the total self magnetic field is shifted upwards, as shown schematically in Fig. 5. In contrast, the self electric field decreases at the inner radius and its magnitude increases at the outer radius of the ring. Thus the self-electric field shifts downwards. As a result of these shifts neither the magnetic nor the electric field are zero at the geometric center of the ring.

When the electron ring is surrounded by a perfect conductor, the shift in the fields discussed above is reduced but additional field components appear as a result of induced charge and current on the conducting wall. For small ring displacements from the center of the minor cross section of the torus, the induced fields vary linearly with the displacement and are identical to those given in Eqs. (10) and (11), for a cylindrical pipe. Quantitative extension of the previous qualitative considerations has shown that the fields at the center of an uniform density electron ring inside a perfectly conducting toroidal chamber of circular cross-section are[5,11]

$$\underset{\sim}{E}_{ind} = -2\pi|e|n_o r_o\left[\left(\frac{r_b^2}{a^2}\frac{\Delta r}{r_o} + \frac{1}{2}\frac{r_b^2}{r_o^2}\ln\frac{a}{r_b}\right)\hat{e}_r + \frac{r_b^2}{a^2}\frac{\Delta z}{r_o}\hat{e}_z\right], \qquad (20)$$

and

$$\underset{\sim}{B}_{ind} = -2\pi|e|n_o\beta_o r_o\left[\frac{r_b^2}{a^2}\frac{\Delta z}{r_o}\hat{e}_r - \left(\frac{r_b^2}{a^2}\frac{\Delta r}{r_o} - \frac{r_b^2}{r_o^2}\left\{1 + \frac{1}{2}\ln\frac{a}{r_b}\right\}\right)\hat{e}_z\right], \qquad (21)$$

where n_o is the ambient density, $\beta_o = v_o/c$, v_o is the azimuthal velocity defined by

$$v_o = \frac{r_o\Omega_{oz}/\gamma_o}{1 + 2(\nu/\gamma_o)(1 + \ln a/r_b)}, \qquad (22)$$

and the displacement $\Delta r, \Delta z$ of the ring from the center of the torus has been assumed to be much less than a. In addition, the fields given by Eqs. (20) and (21) have been derived under the assumption that the angular frequency of the electrons is constant and therefore the electron current density varies proportionally to r.

Using Eqs. (20)-(22), it can be shown that the center of the beam is described by Eqs. (12) and (13) with $\tilde{\omega}_r^2$ and $\tilde{\omega}_z^2$ replaced by

$$\tilde{\omega}_r^2 + \frac{\Omega_{oz}^2}{\gamma_o^2} (\alpha - n^* - n_s r_b^2/a^2), \tag{23}$$

$$\tilde{\omega}_r^2 + \frac{\Omega_{oz}^2}{\gamma_o^2} (n^* - n_s r_b^2/a^2), \tag{24}$$

and

$$\delta P_\theta + \xi \delta P_\theta$$

where

$$\alpha = (1 - \frac{\nu}{\gamma_o} \ell n \frac{a}{r_b}) \xi^2,$$

$$\xi = [1 + \frac{2\nu}{\gamma_o} (1 + \ell n \frac{a}{r_b})]^{-1} \tag{25}$$

and

$$n^* = n\xi.$$

The bounce frequency can be found by substituting Eqs. (23) and (24) into Eq. (18) and is

$$\omega_B^2 = \left(\frac{B_{oz}}{B_{o\theta}}\right)^2 \left(\frac{\Omega_{oz}}{\gamma_o}\right)^2 \left(\alpha - n^* - \frac{n_s r_b^2}{a^2}\right)\left(n^* - n_s \frac{r_b^2}{a^2}\right). \qquad (26)$$

When $n^* = \alpha/2$, for the reasons stated in the paragraphs following Eq. (18), the orbits are closed (stable) as γ_o increases, provided

$$n_s r_b^2/a^2 < \alpha/2$$

or, for $\gamma_o >> 1$

$$I \leq 4.25 \left(\frac{a}{r_b}\right)^2 \left(1 - \frac{\nu}{\gamma_o} \ln \frac{a}{r_b}\right) \gamma_o^3 \ [KA]. \qquad (27)$$

The limiting current given by Eq. (27) is considerably lower than that of Eq. (4) when $B_{o\theta} >> B_{oz}$. In addition, in contrast to the current given by Eq. (4), the current of Eq. (27) is independent of the toroidal magnetic field $B_{o\theta}$.

At this point, it is appropriate to return and discuss further the computer simulation results of Fig. 4. For the 1 KA, 3 MeV beam the $\nu/\gamma_o = 0.0084$. Even at this small value of ν/γ_o toroidal effects are noticeable. The value of ξ computed from Eq. (25) using the above value of ν/γ_o and 6.4 for the ratio a/r_b is 0.95. According to Eqs. (23) and (24) the center of the beam will describe a circle when $\alpha - n^* = n^*$ or for $n = \frac{1}{2}(1 - \nu/\gamma_o \ln a/r_b)\xi = 0.467$, which is in excellent agreement with the simulation. In addition Eq. (26) predicts a period of 188 nsec, which also is in excellent agreement with the simulation.

The most striking manifestation of toroidal effects is in the value of betatron magnetic field required to confine the rotating beam at a specific radius. When the axis of the beam lies along the axis of the torus, i.e., when $\Delta r = \Delta z = 0$, it can be shown from Eqs. (20) and (21) that the external magnetic field required for the beam

to rotate with a radius r_o is

$$B_{oz} = B_o \{1 + 2\nu/\gamma_o (1 + \ell n\, a/r_b)\},$$

where B_o is the magnetic field necessary for a single particle of the same energy to rotate with a radius r_o.

The above expression for the magnetic field is based on the assumption that all the electrons rotate with a constant angular frequency, i.e., the current density increases linearly across the beam. If the current density is constant across the beam, the above expression is slightly modified and becomes

$$B_{oz} = B_o \{1 + 2\nu/\gamma_o (0.5 + \ell n\, a/r_b)\}.$$

For a 10 KA, 2 MeV uniform current density beam with a ratio $a/r_b = 6.4$, the correction is 55%, i.e., $B_{oz}/B_o = 1.55$. This effect is demonstrated clearly by the results of computer simulation shown in Fig. 6. The three snap-shots of the electron ring minor cross section in a modified betatron field correspond to $t = 0$, 20 and 40 nsec. For all practical purposes, the minor radius of the beam remains constant. The external betatron magnetic field is 127 G, i.e., ~ 50% higher than the single particle field. The remaining parameters are summarized in Table II.

Another consequence of the toroidal effects is the increase in the radial displacement of the orbit for fixed energy mismatch and major radius. For $n^* = \alpha/2$ and $n_s r_b^2/a^2 \ll 1$, Eq. (19) becomes $\Delta r_o/r_o = 2(\delta\gamma_o/\gamma_o)\,(1 + \frac{\nu}{\gamma_o}\,\ell n\,\frac{a}{r_b})$. In addition, the ω_B^2 vs. $n_s r_b^2/a^2$ curves of Fig. 3 are shifted to the left and thus the

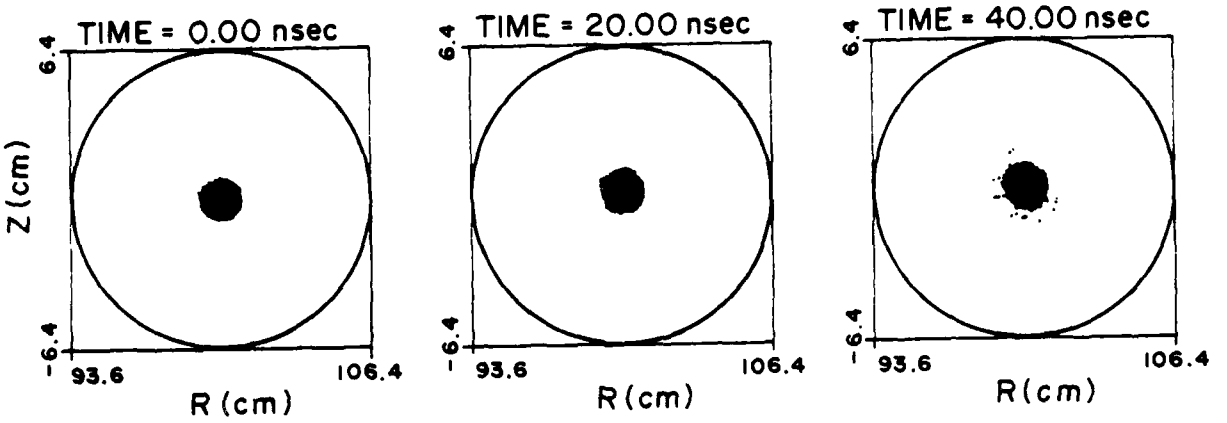

Figure 6. Three snap-shots of the electron ring minor cross section in a modified betatron field. The external magnetic field required to confine the ring is 50% higher than the single particle field. The values of the various parameters in this run are listed in Table II.

Table II.

Parameters of the uniform current density ring	
Beam Energy (MeV)	2
Beam Current (kA)	10
Beam minor radius (cm)	1
Beam major radius (cm)	100
Torus minor radius (cm)	6.4
Vertical magnetic field (G)	127
Toroidal magnetic field (kG)	1.7
External field index	0.25

maximum permissible current that can be accelerated is reduced, as may be seen from Eq. (27).

IV. Acceleration

After injection and trapping the beam is accelerated to high energy by the inductive electric field generated by the time varying betatron magnetic field. As shown in Fig. 7, the acceleration may be divided into three phases

1. Pre-acceleration
2. Diffusion
3. Main acceleration

The pre-acceleration phase occurs for times much shorter than the field diffusion time, i.e., $t \ll t_D = \frac{4\pi}{c^2} \sigma \delta a \ell n \left(\frac{r_o}{a}\right)$, where σ is the conductivity, δ is the thickness, a is the minor radius and r_o the major radius of the torus. During the pre-acceleration phase the self magnetic field of the beam does not have time to diffuse out of the conducting torus. In the example shown in Fig. 7 the total acceleration time was chosen 1 msec and the diffusion time 10 μsec. The ratio of the temporal extent of each phase to the total acceleration time t/t_a is also given in the figure. It is apparent that the beam spends most of its time in the main acceleration phase.

During the pre-acceleration phase the metal wall surrounding the beam can be treated as a perfect conductor. As a result, for small displacement of the beam, the self flux linking the axis of the electron ring remain constant to lowest order. This point is discussed further later.

The condition for the major radius of the electron ring to remain constant can be derived from the conservation of canonical angular momentum

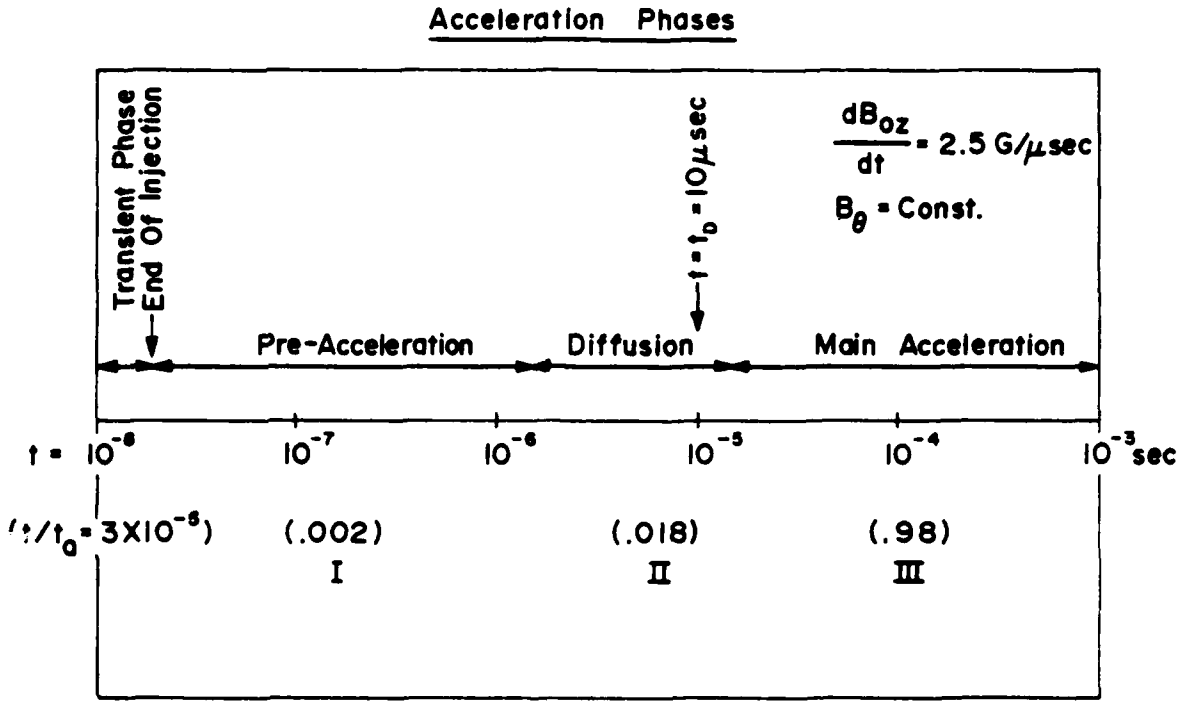

Figure 7. The three phases of acceleration. In the example shown the acceleration time is 1 msec and the diffusion time 10 μsec.

$$P_\theta = m\gamma_o r v_{o\theta} - \frac{e}{c} r\,(A_\theta^{ext} + A_\theta^{s}), \tag{28}$$

where $v_{o\theta}$ is the toroidal velocity, A_θ^{ext} is the vector potential that describes the external magnetic (betatron) field, A_θ^{s} is the vector pote. tial that describes the self magnetic field of the beam and r is the instantaneous radius of the beam.

The self flux linking the ax.s of the ring Φ^s is

$$\Phi^s = 2\pi r A_\theta^{s}, \tag{29}$$

and to lowest order is independent of the beam displacement and thus of time See Eq. (35) . Substituting Eq. (29) into Eq. (28) and using the expression for

$$v_{o\theta} = \frac{r\Omega_{oz}/\gamma_o}{1 + 2\,(\nu/\gamma_o)(1 + \ell n\, a/r_b)},$$

Eq. (28) predicts that r remains constant, provided

$$\frac{\partial}{\partial t}\left[\frac{B_{oz}(t)}{1 + 2\nu/\gamma_o\,(1 + \ell n\, a/r_b)}\right] = \frac{1}{2}\frac{\partial}{\partial t}\langle B^{ext}\rangle. \tag{30}$$

In equation (30), $B_{oz}(t)$ is local magnetic field, ν is the Budker's parameter, a is the minor radius of the torus, r_b is the beam radius and $\langle B^{ext}\rangle$ is the average applied magnetic field.

Using the equation

$$mc^2 \frac{\partial \gamma_o}{\partial t} = -e\vec{v}.\vec{E}, \tag{31a}$$

together with

$$\vec{E} = -\frac{r}{2c}\frac{\partial}{\partial t}\langle \overrightarrow{B^{ext}} \rangle, \tag{31b}$$

equation (30) becomes

$$\frac{\partial B_{oz}(t)}{\partial t} = \frac{1}{2}\left[1 + \frac{2\nu}{\gamma_o^3}\left(1 + \ell n \frac{a}{r_b}\right)\right]\frac{\partial}{\partial t}\langle B^{ext} \rangle. \tag{32}$$

A similar condition has been derived previously[13].

Equation (32) is the condition that must be satisfied in order for the radius of the accelerated electron ring to remain constant. For low ν/γ_o beams, Eq. (32) is reduced to the well known flux rule, i.e.,

$$\frac{\partial B_{oz}(t)}{\partial t} = \frac{1}{2}\frac{\partial}{\partial t}\langle B^{ext} \rangle.$$

The correction term $\frac{2\nu}{\gamma_o^3}\left(1 + \ell n \frac{a}{r_b}\right)$ in Eq. (32) is very sensitive to the beam energy. For a 10 kA, 3 MeV beam injected into a 10 cm minor radius torus with $r_b = 1$ cm, the correction is only 1% and therefore can be neglected. However, when the energy of the same beam is reduced to 0.5 MeV the correction is 48%, i.e., very substantial. The design of the accelerator is simplified considerably by choosing the beam parameters such that the correction term is negligible.

The instantaneous value of $\gamma_o(t)$ may be determined from Eqs. (30) and (31) and for $\gamma_o^2(t) >> 1$ is

$$\frac{\gamma_o(t)}{\gamma_o(0)} = \frac{\left[1 + 2\nu/\gamma_o(0)(1 + \ell n\, a/r_b)\right]}{\left[1 + 2\nu/\gamma_o(t)\,(1 + \ell n\, a/r_b)\right]}\frac{B_{oz}(t)}{B_{oz}(0)}.$$

In contrast to the low current beams, in which $\gamma_o(t)/B_{oz}(t)$ remains approximately

constant during acceleration, for high current beams with toroidal corrections the quantity that remains constant during acceleration is

$$\frac{\gamma_o(t)}{B_{oz}(t)} \left\{1 + 2\nu/\gamma_o(t)\ (1 + \ell n\ a/r_b)\right\} = \text{constant.} \qquad (33)$$

As $\gamma_o(t)$ increases with time, the correction term decreases and Eq. (33) is reduced $\gamma_o(t)/B_{oz}(t) = \text{const.}$

Now, we return to discuss the self flux linking the axis of the ring. In the notation of the toroidal geometry shown in Fig. 8a, the magnetic stream function $\psi = rA_\theta^s$ for $\rho < r_b$ is given, to lowest order, by[11]

$$\psi/Q = 2\ \ell n\ a/r_b + (1 - \rho^2/r_b^2) - 2\ \rho/a\ \frac{\Delta}{a} \cos\ (\psi - \phi) + \frac{\rho}{R_b}\ (\ell n\ \frac{a}{r_b} - \frac{3}{4}\ \frac{r_b^2}{a^2} +$$

$$2 - \frac{5}{4}\ \rho^2/r_b^2)\ \cos\phi, \qquad (34)$$

where $Q = -\text{çeç}\ n_o \pi r_b^2\ \Omega R_b^2/c$, $\Omega = v_\theta/r, \Delta^2 = \Delta r^2 + \Delta z^2$, n_o is the uniform density and it has been assumed that $a << r_o$, $r_b << a$ and Δr, $\Delta z << a$.

The self-flux through the axis of ring is

$$\phi^s = 2\pi\psi(\rho = 0). \qquad (35)$$

Substituting Eq. (34) into Eq. (35), we get

$$\phi^s = 2\pi Q\ (1 + 2\ \ell n\ a/r_b), \qquad (36)$$

which does not depend on the displacement Δr, Δz of the beam. This is a rather

unusal result and deserves further discussion.

To gain some insight into the problem, we have computed the flux linking a horizontal surface s extended from the axis of a straight beam to the inner wall of a perfectly conducting cylinder of circular cross-section as shown in Fig. 8b. The beam displacement is arbitrary but the ratio $r_b/a \ll 1$. It is straight forward to show that the flux through such a surface of length ℓ is

$$\phi^s = (2\ell I/c) \left\{ \ell n\ (a/r_b) - \ell n(1 - \frac{\Delta r^2 + \Delta z^2}{a^2}) \right\} \tag{37}$$

where I is the beam current.

For $(\Delta r^2 + \Delta z^2)^{1/2}/a \ll 1$, Eq. (37) indicates that the flux ϕ^s has a quadratic dependence on the beam displacement. Therefore, since only the linear terms on beam displacement were kept in the derivation of Eq. (34), it is not surprising that the flux given by Eq. (36) is independent of the displacement of the beam.

When the time approaches the magnetic field penetration time t_D, the self magnetic field of the electron beam starts to diffuse out of the finite conductivity metal torus. Using the geometry shown in Fig. 9, it is shown in Appendix A, that for a very thin conductor, i.e., a ≈ b, to lowest order, the self magnetic field of the beam at time t is

$$B_\phi\ (r,t) \approx \frac{2I}{cr} \left[1 - e^{-t/t_D}\right],\ r \geq b \tag{38}$$

$$B_\phi\ (r,t) \approx \frac{2I}{cr},\ r_b \leq r \leq a,$$

where

$$t_D \approx \frac{4\pi\sigma\delta a}{c^2}\ \ell n\ (\frac{r_o}{a}).$$

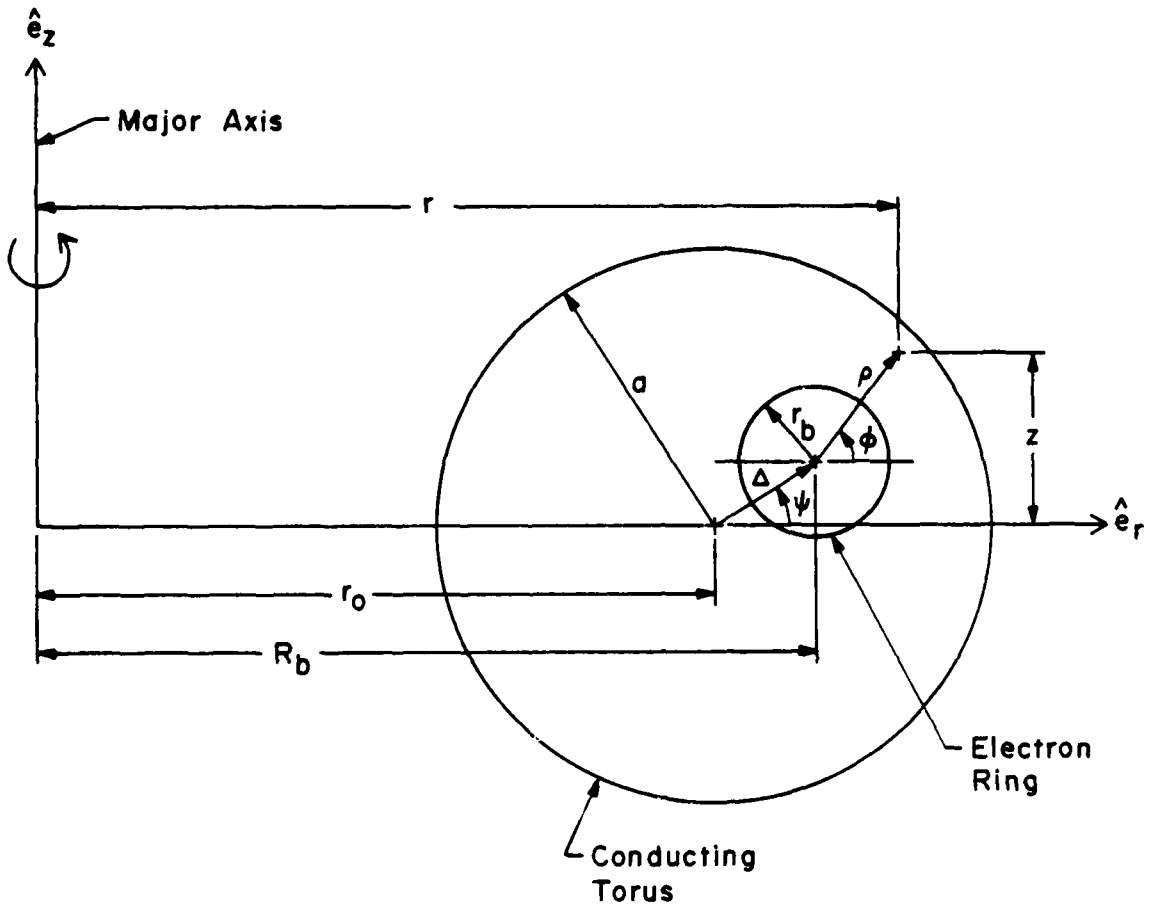

Figure 8a. System of coordinates for Eq. (34).

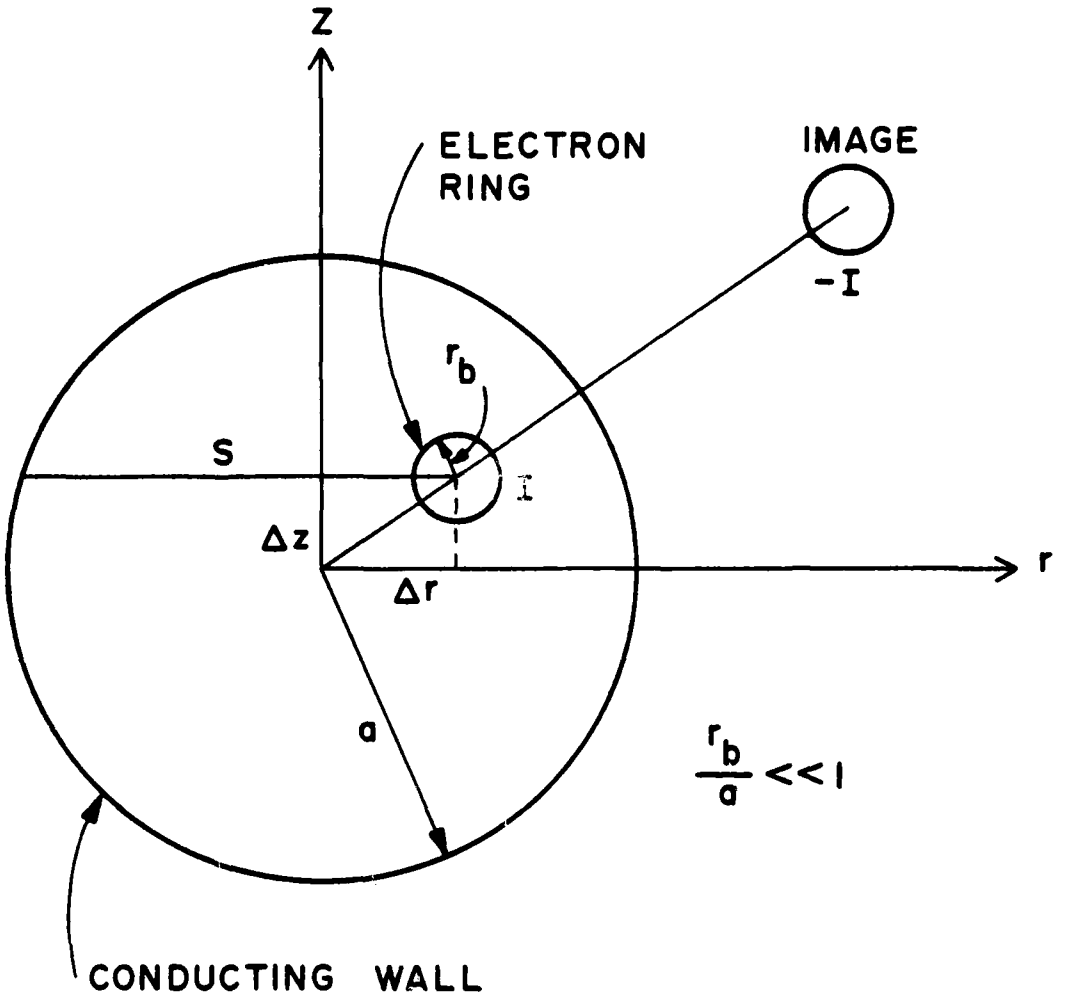

Figure 8b. A displaced straight electron beam inside a perfectly conducting pipe. The image current is located at a distance $a^2/(\Delta r^2 + \Delta z^2)^{1/2}$ from the center of the pipe.

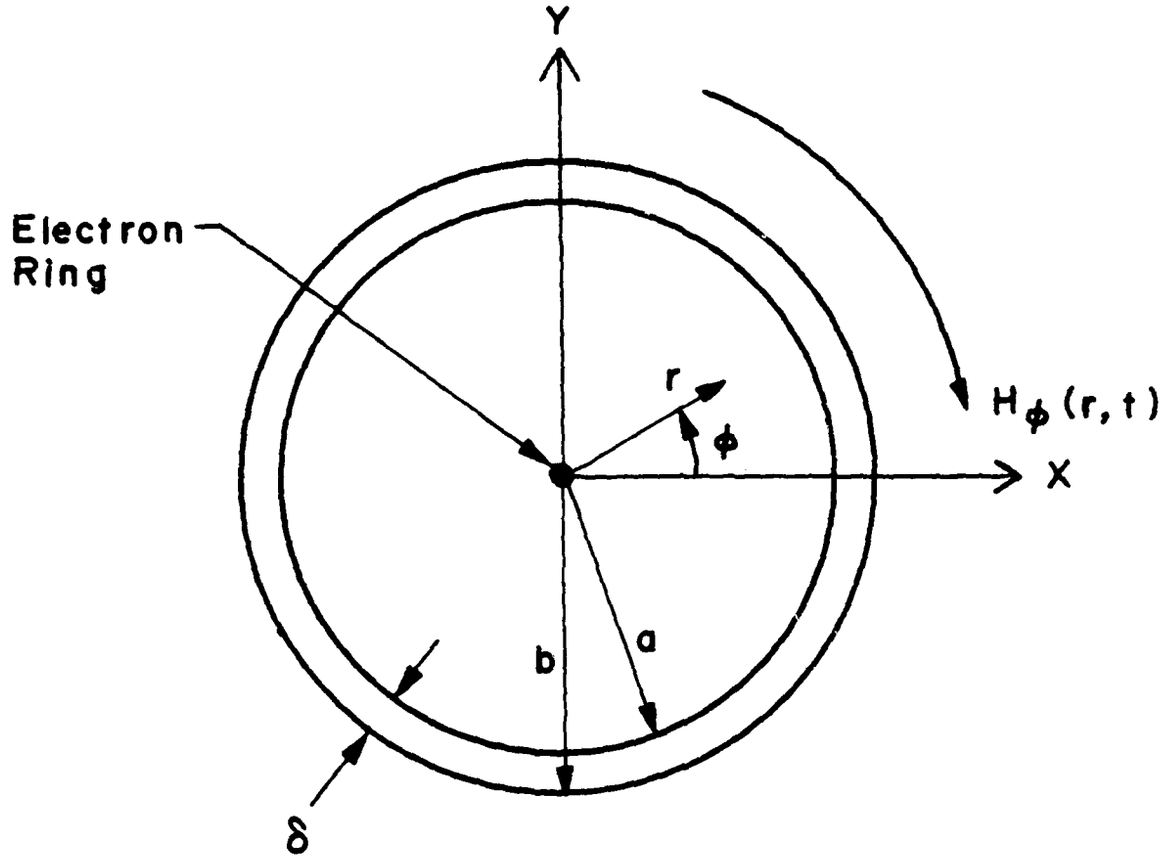

Figure 9. System of coordinates used to compute the magnetic field during diffusion.

These equations are based on the assumption

that $\delta/a \ll 1$, $\left((\delta/b)\ell n \frac{r_o}{b}\right)^{1/2} \ll 1$ and the inductive electric field varies

as $E_z(r,t) = \frac{b}{c} \frac{\partial B_\phi(b,t)}{\partial t} \ell n \left(\frac{r}{r_o}\right)$, i.e., goes to zero at $r = r_o$ (pseudo-toroidal

geometry).

The self magnetic flux in the three regions is given by

$$\phi^s = \begin{cases} \frac{4\pi r_o}{c} I \ell n(a/r_b) & r \leq a \\ 0 & a \leq r \leq b \\ \frac{4\pi r_o}{c} I \left[1 - e^{-t/t_D}\right] \ell n \frac{r_o}{b} & r \geq b \end{cases}$$

and it diffuses out at the rate

$$\frac{d\phi^s}{dt} = \frac{4\pi r_o I}{t_D c} e^{-t/t_D} \ell n \left(\frac{r_o}{b}\right). \tag{39}$$

The inductive electric field generated by the changing flux given in Eq. (39) acts to slow down the beam. In addition, for a constant current density ring, the hoop stresses increase by the ratio $(2 + \ell n \frac{8r_o}{e r_b})/(1 + \ell n \frac{a}{r_b})$, and the induced magnetic field components go to zero at the end of the diffusion. However, the electric field components remain the same. As a result, for a electron ring that is situated along the minor axis of the torus, the decrease in its equilibrium radius associated with the reduction of γ_o is greater than the corresponding increase of

the equilibrium radius associated with the enhanced hoop stresses and thus equilibrium can be lost. This difficulty can be avoided by placing a set of external conductors along the minor cross-section of the torus having a poloidal distribution that closely resembles the distribution of wall currents in a perfect conductor, i.e.,

$$I_w = -\frac{I_b}{2\pi a}\left[1 - \frac{a}{2r_0}\cos\phi\right],$$

where I_w is the wall current per unit length and I_b the ring current.

This compensation is satisfactory even when the beam is displaced off center and rotates around the equilibrium position with ω_B, provided that $\omega_B\tau_D >> 1$. The reason is that the correction term in the fields at the center of the ring,[14] when the skin depth is much greated than the thickness of the conductor, is

$$\frac{-2\,e^{-t/\tau_D}}{\omega_B\tau_D}\sin\omega_B t,$$

and therefore, it can be neglected. Similarly, when the skin depth is much smaller than the thickness, the correction term is also small and is given by

$$\sqrt{\frac{2(b-a)/a}{\omega_B\tau_D}} + \frac{2\,e^{-t/\tau_D}}{\omega_B\tau_D}\sin\omega_B t.$$

In addition, we have shown that the components of magnetic field that are proportional to the displacement of the beam do not diffuse out of the chamber when $\omega_B\tau_D >> \gamma_o^2$. As a consequence $n_s r_b^2/a^2$ does not increase during diffusion and ω_B does not change polarity. Therefore, the drug instability[14] can be avoided by choosing the various parameters to give $\omega_B > o$ at the commencement of the diffusion process.

During the main acceleration phase the significance of toroidal effects is reduced because $\nu/\gamma_o \to o$. When B_θ remains approximately constant as shown in Fig. 10, or increases with time the accelerated beam moves closer to the center of the minor cross-section of the torus. This may be seen from the beam equations, which for $B_{o\theta}$ = const., are:

$$\Delta\ddot{r} + (\dot{\gamma}/\gamma)\ \Delta\dot{r} + \tilde{\omega}_r^{\,2}\Delta r = (\Omega_{o\theta}/\gamma)\ \Delta\dot{z} + \frac{\Omega_{oz}}{\gamma}\frac{\langle\delta P_\theta\rangle}{\gamma m r_o}, \tag{40}$$

$$\Delta\ddot{z} + (\dot{\gamma}/\gamma)\Delta\dot{z} + \tilde{\omega}_z^{\,2}\Delta z = -(\Omega_{o\theta}/\gamma)\Delta\dot{r}. \tag{41}$$

With the exception of the second term $(\dot{\gamma}/\gamma)\Delta\dot{r}$, Eqs. (40) and (41) are identical to Eqs. (12) and (13). For n = 1/2, Eqs. (40) and (41) can be readily solved. Introducing a new variable $\psi = \Delta r + i\Delta z$, these two equations can be combined into a single equation

$$\ddot{\psi} + \frac{1}{\gamma}(\dot{\gamma} + i\Omega_{o\theta})\ \psi + \omega_o^{\,2}\psi = \frac{\Omega_{o\theta}}{\gamma}\frac{\langle\delta P_\theta\rangle}{\gamma m r_o}, \tag{42}$$

where $\omega_o = \tilde{\omega}_r^{\,2} = \tilde{\omega}_z^{\,2}$. The general solution of Eq. (42) is

$$\psi = \psi_1 + \psi_2 + \psi_p$$

where

$$\psi_1 = \frac{a_1\, e^{-i\int_o^t \omega_+^{(o)}dt'}}{\gamma^{1/2}\left[\left(\frac{\Omega_{o\theta}}{\gamma}\right)^2 + 4\omega_o^{\,2}\right]^{1/4}},$$

$$\psi_2 = \frac{a_2 e^{-i\int_o^t \omega_-^{(o)}dt'}}{\gamma^{1/2}\left[\left(\frac{\Omega_{o\theta}}{\gamma}\right)^2 + 4\omega_o^{\,2}\right]^{1/4}}$$

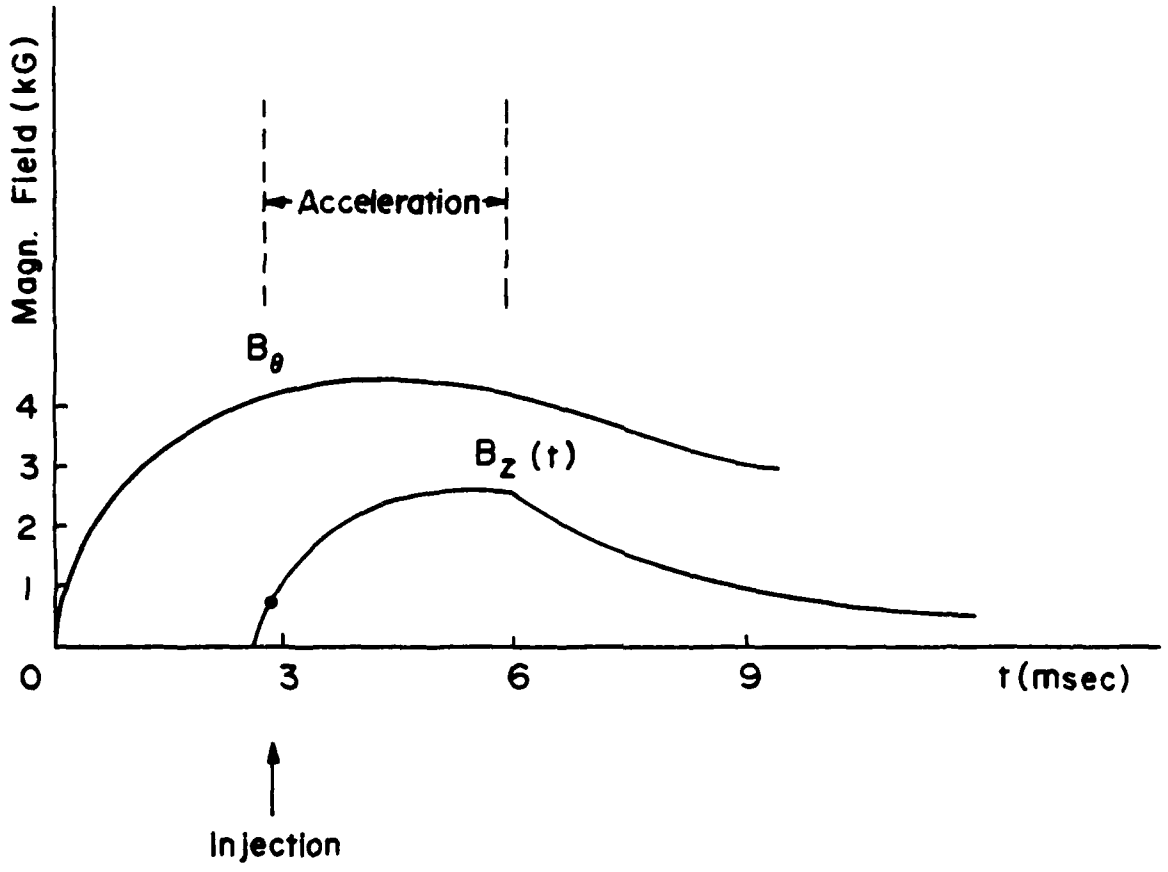

Figure 10. This figure illustrates a possible time dependence of the toroidal and betatron fields. From the stability point of view other time variations are more appropriate.

and

$$\psi_p = \psi_1 \int_o^t \frac{(-\frac{\Omega_{o\theta}}{\gamma}\frac{\langle \delta P_\theta \rangle}{\gamma m r_o}\psi_2)\,dt'}{w(\psi_1, \psi_2)} + \psi_2 \int_o^t \frac{(\frac{\Omega_{o\theta}}{\gamma}\frac{\langle \delta P_\theta \rangle}{\gamma m r_o})\,\psi_1\,dt'}{w(\psi_1, \psi_2)} .$$

In the above equations $\omega_{\pm}^{(0)} = \frac{\Omega_{o\theta}}{2\gamma} \pm \sqrt{(\frac{\Omega_{o\theta}}{2\gamma})^2 + \omega_o^2}$ and $w(\psi_1, \psi_2)$ is the Wronskian of the two independent solutions ψ_1 and ψ_2 of the homogeneous equation.

Since the denominator of ψ_1 and ψ_2 increases, when the betatron field increases in time, the center of the beam moves toward the center of the minor cross-section of the torus during the acceleration.

V. Grad B Drift in the Modified Betatron

Until now we have neglected in our analysis the radial gradient in the toroidal magnetic field, B_θ. In this section we consider carefully the effect of this non-linearity on particle motion, assuming that it is the dominant non-linear effect.

The linearized equations of motion of a particle located at $r = r_o + \Delta r + \delta r$, $z = \Delta z + \delta z$ where Δr and Δz are the beam position with respect to the center of the torus (See Figure 11) are

$$\begin{aligned} \ddot{r}_1 + (1-n)\,\tilde{\Omega}_{zo}^2\, r_1 - n_s \tilde{\Omega}_{zo}^2\,(\delta r + \frac{r_b^2}{a^2}\Delta r) &= \tilde{\Omega}_{\theta o}(1 - \frac{r_1}{r_o})\,\dot{z}_1 + \tilde{\Omega}_{zo}\frac{\delta P_\theta}{\gamma_o m r_o}, \\ \ddot{z}_1 + n\tilde{\Omega}_{zo}^2\, z_1 - n_s \tilde{\Omega}_{zo}^2(\delta z + \frac{r_b^2}{a^2}\Delta z) &= -\tilde{\Omega}_{\theta o}(1 - \frac{r_1}{r_o})\,\dot{r}_1, \end{aligned} \qquad (43)$$

where

$$r_1 = \Delta r + \delta r,$$

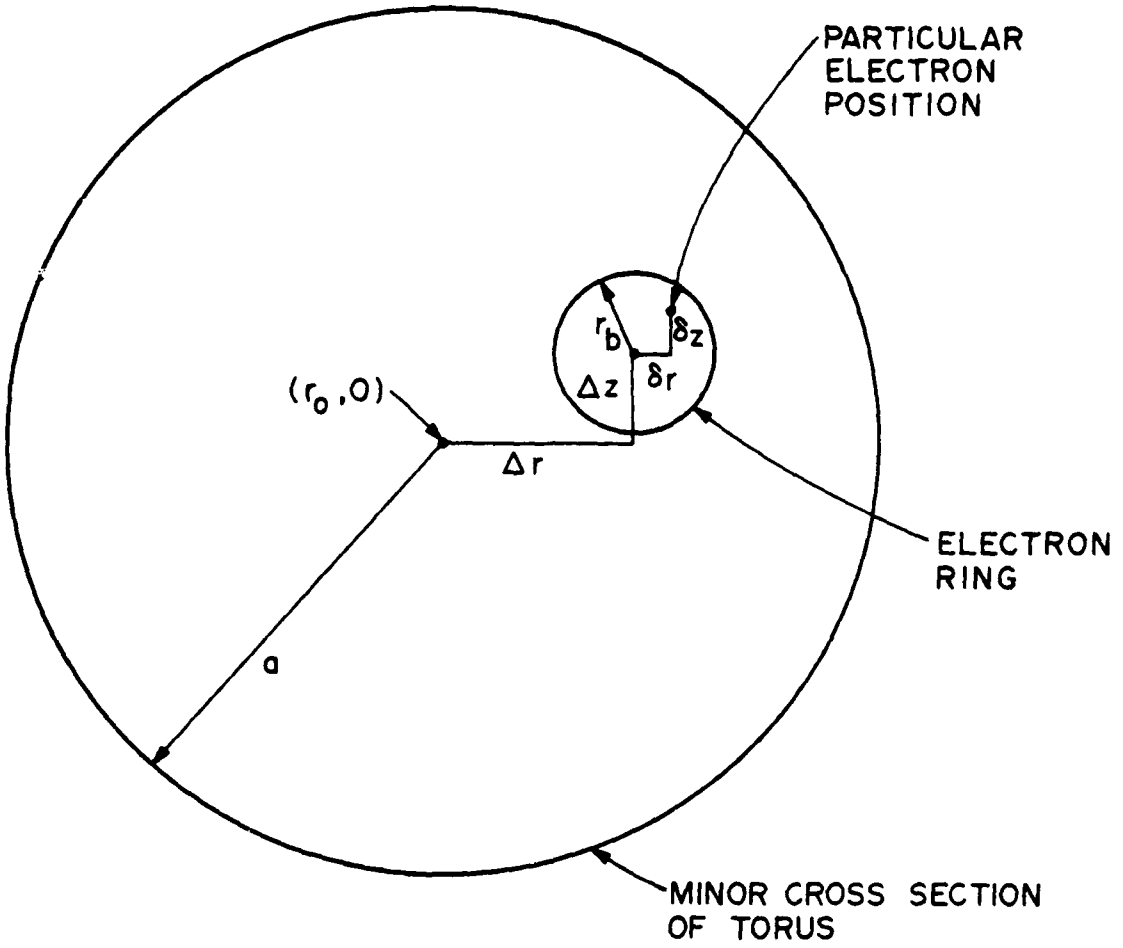

Figure 11. System of coordinates used to analyze the drift resulting from the gradient in the toroidal magnetic field.

$$z_1 = \Delta z + \delta z,$$

$$\tilde{\Omega}_{zo} = \Omega_{oz}/\gamma_o,$$

$$\tilde{\Omega}_{\theta o} = \Omega_{o\theta}/\gamma_o.$$

Choosing $n = \frac{1}{2}$ simplifies the subsequent analysis. Making this choice and defining $\psi = r + iz$ gives

$$\ddot{\psi}_1 + \frac{1}{2}\tilde{\Omega}_{zo}^2\,\psi_1 - n_s\tilde{\Omega}_{zo}^2(\delta\psi + \frac{r_b^2}{a^2}\Delta\psi)$$

$$= -i\tilde{\Omega}_{o\theta}(1 - \frac{Re\psi_1}{r_o})\,\dot{\psi}_1 + \tilde{\Omega}_{zo}\frac{\delta P_\theta}{\gamma_o m r_o} \qquad (44)$$

We proceed to solve (44) perturbatively, assuming $Re\psi_1 << r_o$.

The zero order equation, neglecting the non linearity, is easily solved. First an average is performed over initial positions and velocities of the particles to obtain a single equation governing the motion of the beam center, $\Delta\psi$. Denoting this average by brackets we will have $\langle\delta\psi\rangle = 0$ by definition and, it may be shown that as long as no kinks develop in the beam $\langle\delta\dot{\psi}\rangle = 0 = \langle\ddot{\delta\psi}\rangle$. Once the averaged equation is obtained it may be subtracted from (44) to obtain an equation for $\delta\psi$. Carrying out

this program, we find for the zero order solution:

$$\Delta\psi^{(0)} = \frac{\langle \delta P_\theta \rangle}{\hat{\Omega}_{zo}\ \gamma_o m r_o\ (\frac{1}{2} - \frac{r_b^2}{a^2} n_s)} + Ae^{-i\omega_1 t} + Be^{i\omega_2 t},$$

$$\delta\psi^{(0)} = \frac{\delta P_\theta - \langle \delta P_\theta \rangle}{\hat{\Omega}_{zo}\ \gamma_o m r_o\ (\frac{1}{2} - n_s)} + Ce^{-i\omega_3 t} + De^{-i\omega_4 t}, \tag{45}$$

where A, B, C, and D are arbitrary complex constants and where the frequencies $\omega_1 \cdots \omega_4$ are given by

$$\omega_{1,2} = \frac{1}{2}\left[\hat{\Omega}_{\theta o} \pm \left(\Omega_{\theta o}^2 + 4\hat{\Omega}_{zo}^2\ (\frac{1}{2} - \frac{r_b^2}{a^2} n_s)\right)^{\frac{1}{2}}\right],$$

$$\omega_{3,4} = \frac{1}{2}\left[\hat{\Omega}_{\theta o} \pm \left(\hat{\Omega}_{\theta o}^2 + 4\hat{\Omega}_{zo}^2\ (\frac{1}{2} - n_s)\right)^{\frac{1}{2}}\right].$$

We shall take subscripts 1 and 3 to correspond to the + signs.

In writing (45) we have assumed that neither $(\frac{1}{2} - \frac{r_b^2}{a^2} n_s)$ nor $(\frac{1}{2} - n_s)$ is zero. If either of these quantities does vanish (corresponding physically to the vanishing of net radial restoring forces) the corresponding solutions to (44) grow secularly, indicating a curvature or centrifugal drift in the vertical direction. Below we assume that the radial restoring forces do not vanish for either beam or particle motion. In addition we shall make the assumption that $\langle \delta P_\theta \rangle = 0$. This is the same as the requirement that the equilibrium position of the beam be at the center of the minor cross section of the torus. This assumption has no effect whatsoever on the basic physical results and conclusions but does simplify the mathematics somewhat.

We may return to (44) and calculate the first order correction to the beam position, $\Delta\psi^{(1)}$. The equation to be solved is

$$\Delta\ddot{\psi}^{(1)} + i\tilde{\Omega}_{\theta o}\Delta\dot{\psi}^{(1)} + \tilde{\Omega}_{zo}{}^{2}\left(\frac{1}{2} - \frac{r_b^{\,2}}{a^2} n_s\right)\Delta\psi^{(1)} = i\frac{\tilde{\Omega}_{\theta o}}{r_o}\left\langle\left[\mathrm{Re}\,\psi_1^{(o)}\right]\dot{\psi}_1^{(o)}\right\rangle. \tag{47}$$

Substituting from (45) we find the right hand side of (47) is

$$\left\langle\left[\mathrm{Re}\,\psi_1^{(0)}\right]\dot{\psi}_1^{(0)}\right\rangle = -i\sum_{j=1}^{2}\sum_{k=1}^{2}\omega_j\,\rho_j\,\rho_k e^{-i(\omega_j t - \alpha_j)}\cos(\omega_k t - \alpha_k) - \frac{i}{2}\sum_{j=3}^{4}\omega_j\langle\rho_j^2\rangle, \tag{48}$$

where we have defined

$$A,\ B,\ C,\ D \equiv \rho_j e^{i\alpha_j};\ j = 1,\ 2,\ 3,\ 4,$$

and where we have assumed that

$$\langle C\rangle = \langle D\rangle = 0.$$

From (47) and (48) we can see that apart from oscillating terms the net effect of the radial gradient in B_θ is to cause an outward shift in the equilibrium position of the beam:

$$\Delta\psi_1^{(1)} = \frac{\left(\frac{\tilde{\Omega}_{\theta o}}{2r_o}\right)\left\langle\sum_{j=1}^{4}\omega_j\rho_j{}^{2}\right\rangle}{\tilde{\Omega}_{zo}{}^{2}\left(\frac{1}{2} - \frac{r_b^{\,2}}{a^2} n_s\right)} + \text{oscillating terms.} \tag{49}$$

This result is simply understood as the result of a balance between the outward, "diamagnetic" force (which tends to expel the beam from the high field region) and the inward radial restoring force.

Since the ρ_j values in (49) depend on the details of the injection process, it is difficult to draw practical, quantitative conclusions from this result. However it is probably safe to conclude quite generally that any device should be designed so that $\frac{1}{2} >> \frac{r_b^2}{a^2} n_s$ for all times, or

$$\nu/\gamma_o << \frac{1}{4} (\gamma_o \hat{\Omega}_{zo} a/c)^2, \tag{50}$$

for the case of a perfectly conducting wall. The γ_o should be omitted in the parentheses on the right hand side of (50) in the case of a poorly conducting wall (diffusion time short compared to a beam oscillation period). We note that the constraint in (50) is independent of the strength of the toroidal magnetic field.

Two dimensional computer simulations bear out our claim that self consistent beam equilibria exist in the presence of a gradient in B_θ, as long as the net radial focusing forces (proportional, basically, to the denominator in (49) but generalized to include the case $n \neq \frac{1}{2}$, and to include toroidal corrections to the self fields) do not vanish. In Figure 12 we show a succession of "snapshots" of a beam cross section, which remains in its equilibrium position for significant times compared to r_b/V_D, where V_D is the single particle drift velocity,

$$V_D = \Omega_{\theta o} \rho^2/2r_o,$$

and where ρ is a particle gyradius. No drift is observed. (This is not just a

I_b = 10 kA E_b = 3 MeV

r_o = 100 cm a = 6.4 cm r_b = 1 cm

B_z = 160 G B = 1.4 kG n = 0.3

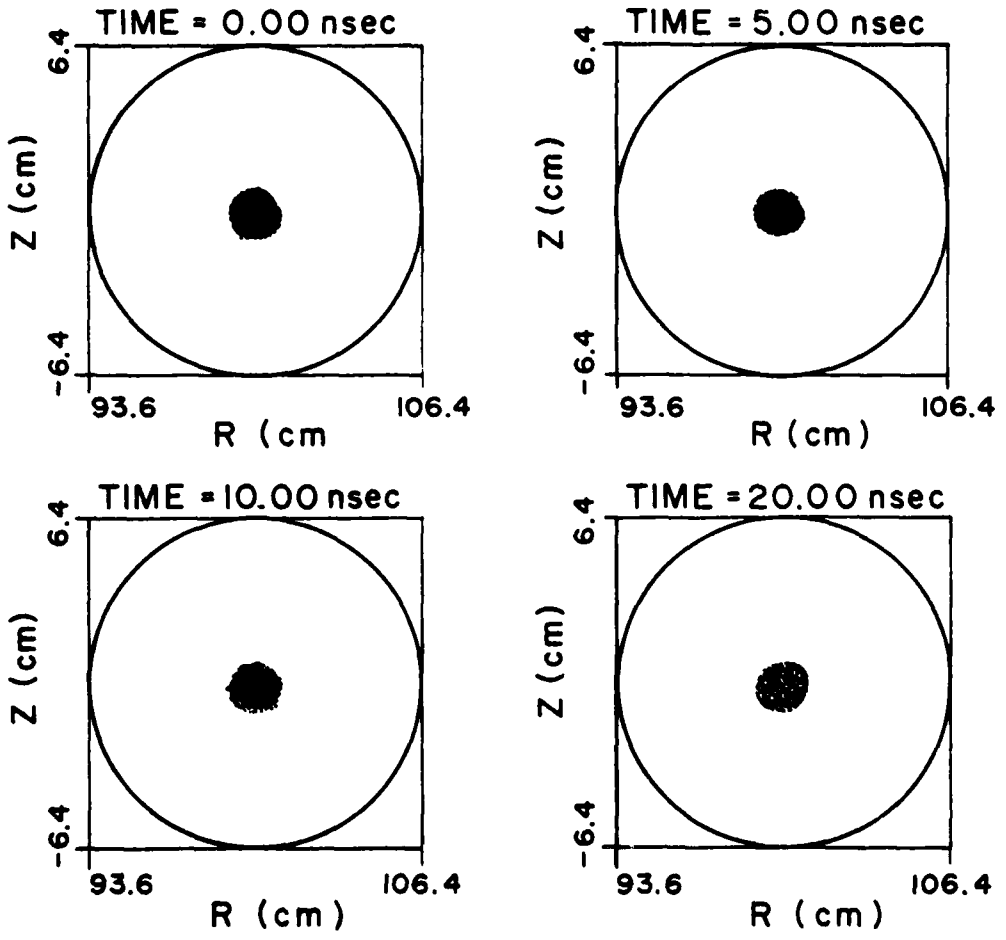

Figure 12. Four snap-shots of the electron ring minor cross-section. The values of the various parameters used in this computer simulation run are shown at the top of the figure.

visual observation but is obtained from a plot of average particle position vs. time.)

In Figure 13, on the other hand, we present a case in which net radial focusing does nearly vanish. Loss of confinement is extremely rapid under such conditions. The ring drifts vertically with an average speed of 0.25 cm/nsec.

VI. The Effect of Emittance

Up to this point, we have dealt with the equations describing the motion of the center of an electron ring in a modified betatron configuration. In this section, we discuss the effect of the finite emittance on the equilibrium of the gyrating electron ring using the beam envelope equation. When the major beam radius r_o is large, $n = \frac{1}{2}$, γ_o = constant, $\frac{\nu}{\gamma} \ll 1$, the energy mismatch $\delta\gamma_o = 0$ and the effect of surrounding walls is neglected, the beam envelope equation in the paraxial approximation for $B_{o\theta} \gg B_{oz}$ becomes[13] in the Larmor frame of reference.

$$r_b''(s) + \frac{1}{r_o^2}\left(\frac{B_{o\theta}}{2B_{oz}}\right)^2 r_b(s) - \frac{2\nu/\gamma_o^3}{\beta_o^2 r_b(s)} - \frac{\varepsilon^2}{r_b^3(s)} = 0, \qquad (51)$$

where ε is the beam emittance (unnormalized), $s = \theta r_o$ is the length along the minor axis of the torus and $r_b'(s) \equiv dr_b/ds$. For a zero emittance beam the motion of the particles is laminar and the equilibrium is called either laminar flow or Brillouin

I_b = 10 kA E_b = 3 MeV

r_o = 100 cm a = 6.4 cm r_b = 1 cm

B_z = 150 G B = 1.4 kG n = 0.3

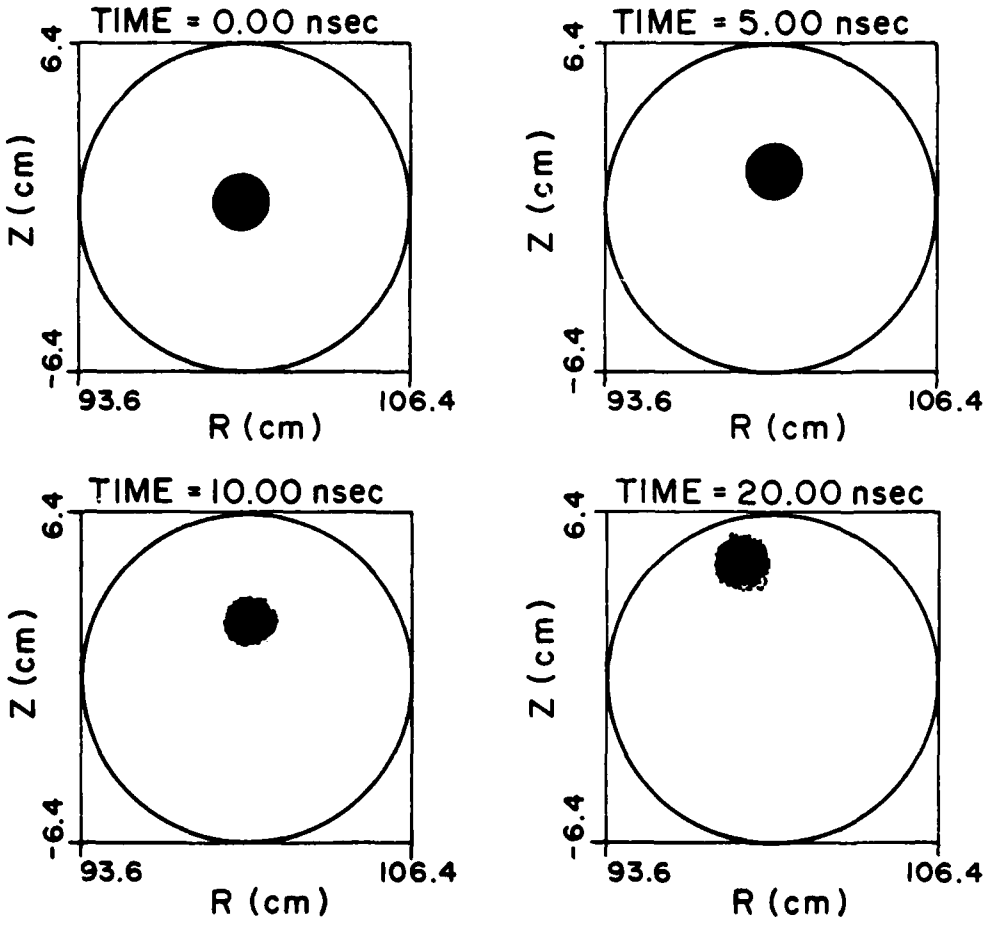

Figure 13. Reducing the betatron field by 10 G, but keeping the remaining parameters fixed, as in the run of Figure 12, the electron ring drifts rapidly in the vertical direction.

flow. The equilibrium radius in this case is obtained from Eq. (51) by setting

$$r_b'' = \varepsilon = 0$$

and is

$$r_{b,eq}^{\ell} \simeq \frac{2c}{\Omega_{o\theta}} \left(\frac{2\nu}{\gamma_o}\right)^{\frac{1}{2}}, \tag{52}$$

when $\gamma_o \gg 1$. For a finite emittance beam, the equilibrium radius can be determined from Eq. (51) by taking $r_b''(s) = 0$ and is

$$r_{b,eq} = \frac{2c}{\Omega_{o\theta}} \left\{\frac{\nu}{\gamma_o} + \left[\left(\frac{\nu}{\gamma_o}\right)^2 + \varepsilon^2 \left(\frac{\Omega_{o\theta}\gamma_o}{2c}\right)^2\right]^{\frac{1}{2}}\right\}^{\frac{1}{2}}. \tag{53}$$

For small envelope oscillations $r_b = r_{b,eq} + \delta$, with $\delta/r_{b,eq} \ll 1$ and Eq. (51) gives

$$\delta'' + 2\left[(\Omega_{o\theta}/2\gamma_o c)^2 + \varepsilon^2/r_{b,eq}^4\right]\delta = 0,$$

that has a period

$$T = \frac{2\pi/c}{\left\{2\left[(\Omega_{o\theta}/2\gamma_o c)^2 + 3\ \varepsilon^2/r_{b,eq}^4\right]\right\}^{1/2}}. \tag{54}$$

The effect of emittance on the equilibrium of the ring has been studied extensively using a computer simulation code. Numerical results from the computer simulation are given in Figs. 14 to 17. For a beam with $\gamma_o = 7$, $I = 10$ KA, $r_o = 100$ cm, $B_{oz} = 160$G, $B_{o\theta} = 1415$G, Eq. (52) predicts that the equilibrium radius for the Brilluin flow is 1 cm. The numerical results of Fig. 14 give also a radius of 1 cm, that for all practical purposes remains constant in time. In this run the

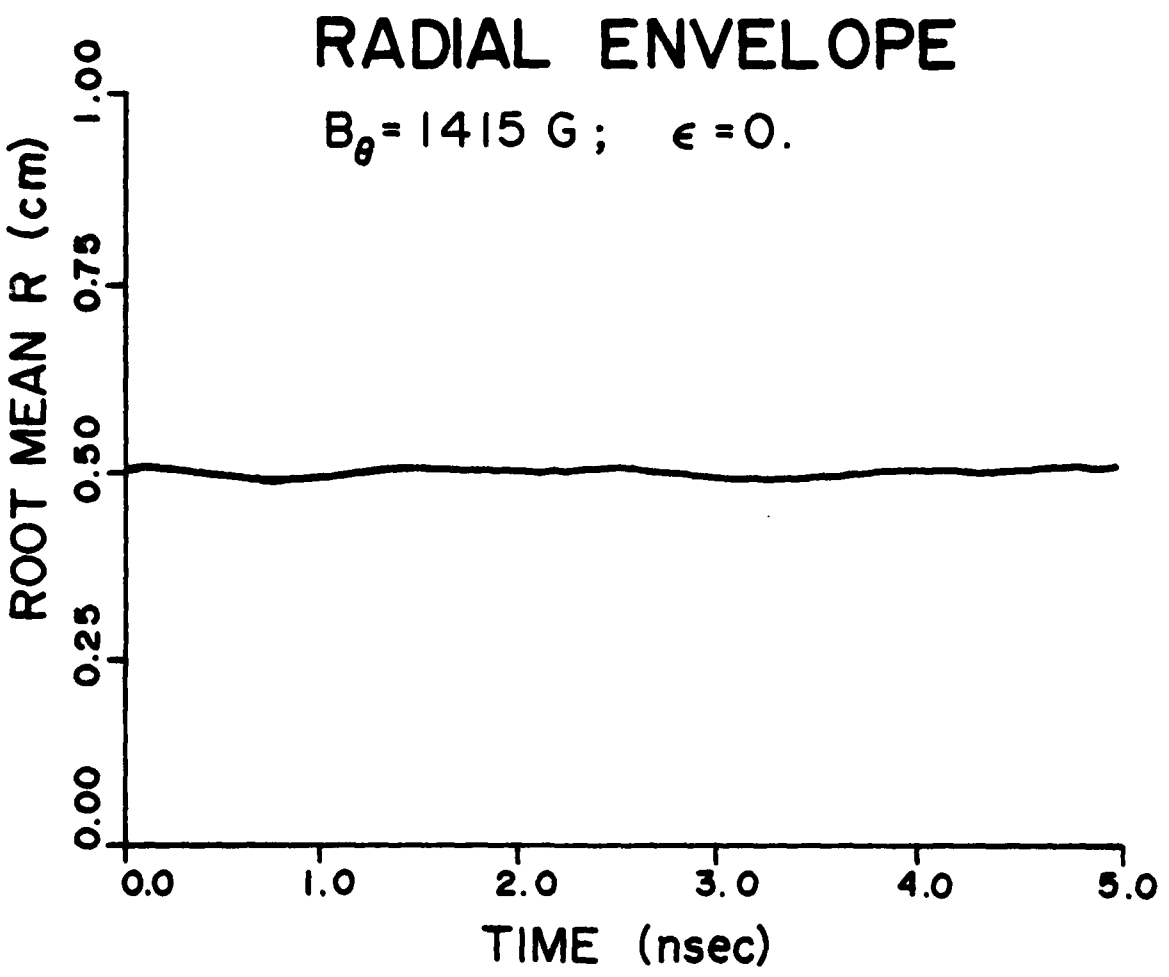

Figure 14. Root-mean distance of the electrons from the center of the ring as a function of time, when the emittance, ϵ, is zero.

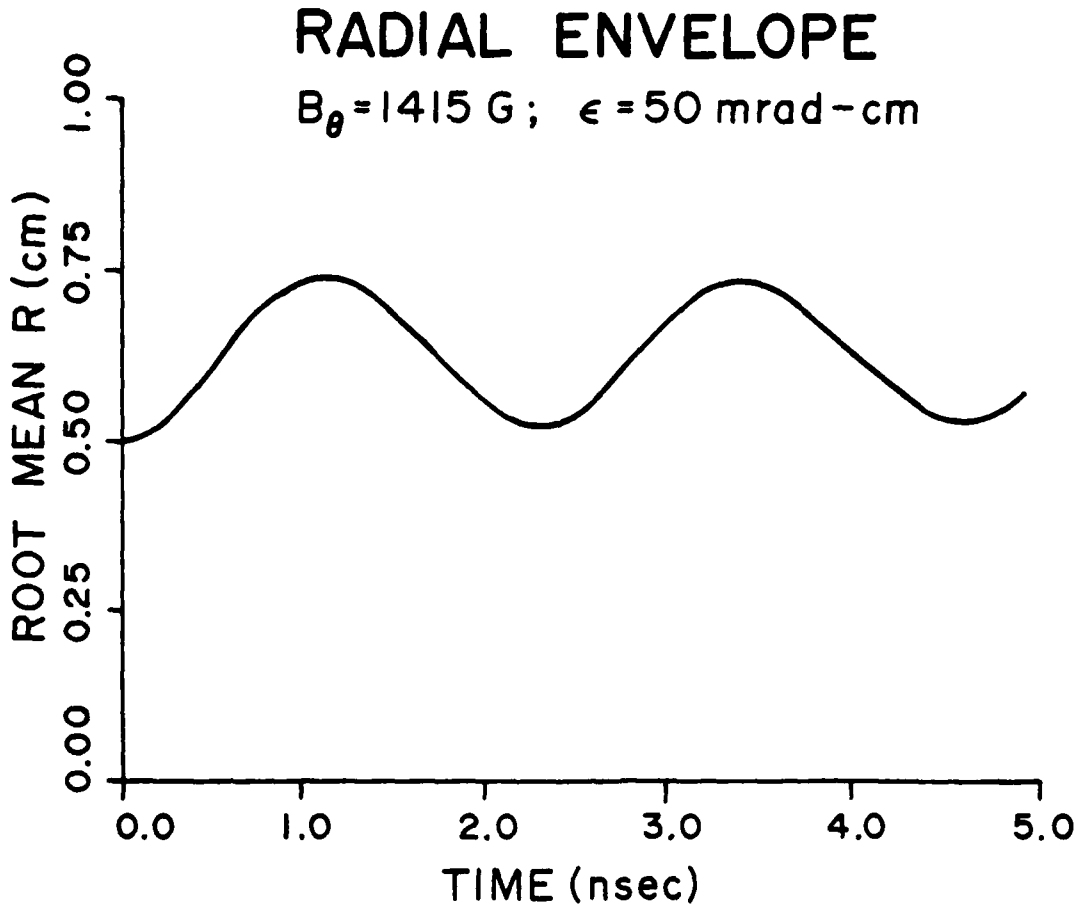

Figure 15. Root-mean distance of the electron from the center of the ring as a function of time. In this run ϵ = 50 mrad-cm.

RING CROSS SECTION

B_θ = 1415 G; ϵ = 50 mrad-cm

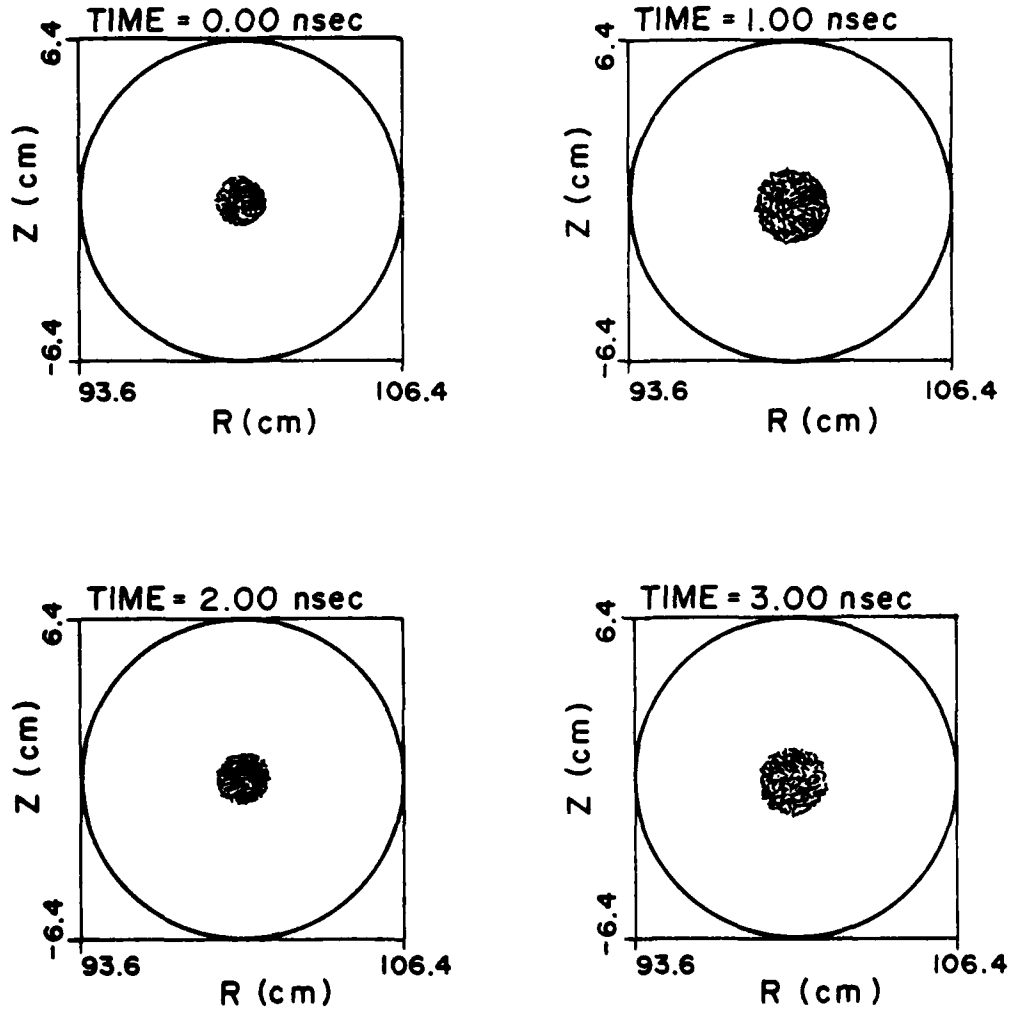

Figure 16. Four snap-shots of the electron ring minor cross-section when ϵ = 50 mrad-cm.

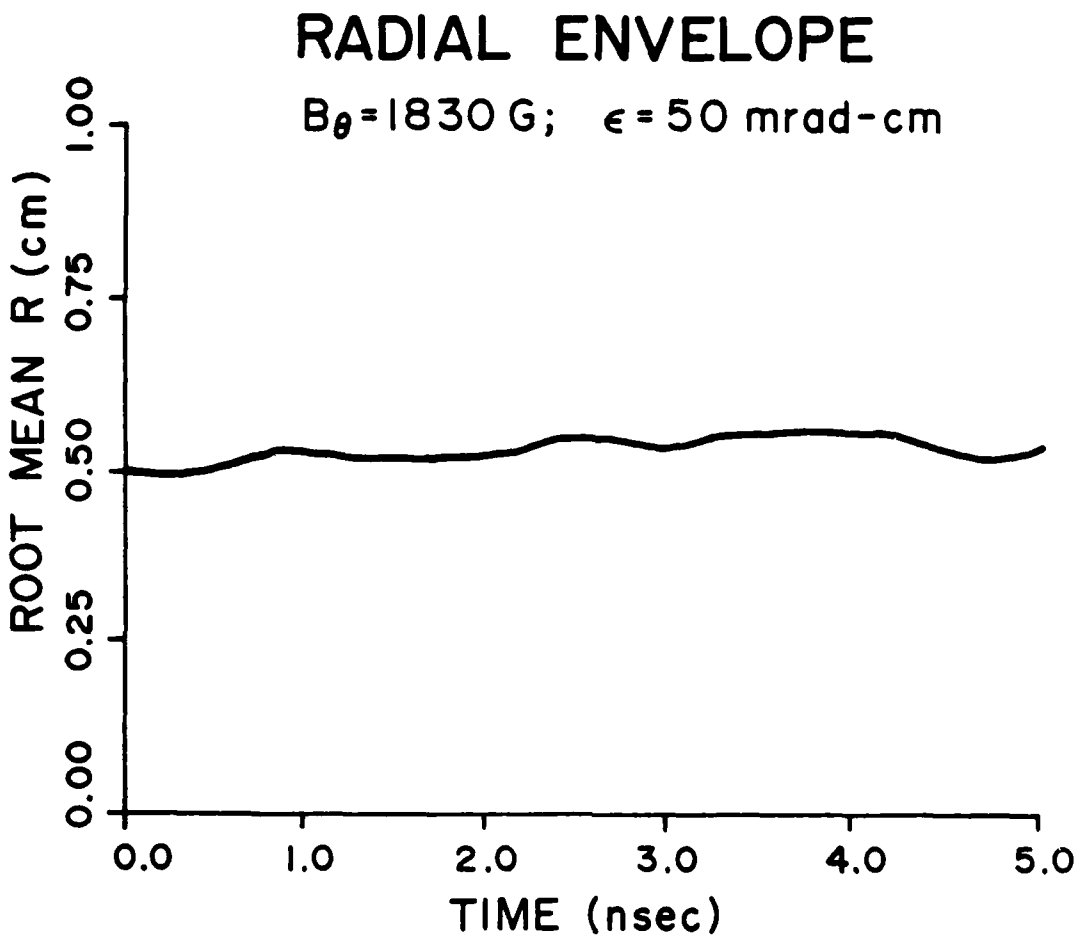

Figure 17. Root-mean distance of the elctrons from the center of the ring. The envelope oscillations are drastically reduced when the toroidal magnetic field is increased from 1415 G to 1830 G.

electron beam is injected into the torus with a rotational frequency that is half of the local cyclotron frequency. Figure 15 shows the envelope in time of a non-rotating beam. The various parameters in this run have the same values as those in Fig. 14, except now the emittance is non-zero in the Larmor frame. For the equivalent emittance of ϵ = 50 mrad-cm, Eq. (53) gives an $r_{b,eq}$ = 1,21 cm and the numerical results 1.24 cm. Similarly, Eq. (54) gives period of 2.13 nsec and the numerical results 2.28 μsec. Snap shots of the beam cross-section from the same run are given in Fig. 14. The oscillations observed in the run of Fig. 15 can be avoided by "matching" the beam, i.e., by raising the $B_{o\theta}$ magnetic field to 1830G. This value of magnetic field gives an $r_{b,eq} \approx 1$ cm, which is the radius of the beam for Brillouin flow. Numerical results from this run are shown in Fig. 17.

The electron beams discussed so far in this section were monoenergetic with finite emittance. Such beams have an axial velocity spread equivalent to that of a cold beam with energy spread $\Delta\gamma$ that is given by[15]

$$\frac{\Delta\gamma}{\gamma} = \frac{1}{2}\left(\frac{\gamma\beta\epsilon}{r_b}\right)^2.$$

Actual or equivalent energy speed in the direction of beam propagation has an important effect on the dynamics of electrons as may be seen as follows. The equations describing the motion of individual electrons in cylindrical geometry are identical with those describing the motion of the center of the beam, provided that $\tilde{\omega}_r^2$ and $\tilde{\omega}_z^2$ are replaced by

$$\tilde{\omega}_r^2 = \left(\frac{\Omega_{oz}}{\gamma_o}\right)^2 (1 - n - n_s),$$

$$\tilde{\omega}_z^2 = \left(\frac{\Omega_{oz}}{\gamma_o}\right)^2 (n - n_s),$$

and

$$\frac{\langle \delta P_\theta \rangle}{\gamma_o m r_o} = \frac{c^2}{r_o \Omega_{oz}} \frac{\Delta\gamma}{\gamma_o} .$$

The above set of equations are based on the assumption that toroidal effects can be neglected. In addition, it should be emphasized that $\Delta\gamma$ is thermal energy spread and not the energy mismatch $\delta\gamma_o$ discussed in Section III.

For $n = \frac{1}{2}$, the solution of the individual particle equations are

$$r - r_o = \delta r_o \cos\omega_B t - \delta z_o \sin\omega_B t + r_o \frac{\Delta\gamma}{\gamma_o} \frac{(1 - \cos\omega_B t)}{\frac{1}{2} - n_s}, \qquad (55)$$

$$\delta z = \delta z_o \cos\omega_B t + \delta r_o \sin\omega_B t - r_o \frac{\Delta\gamma}{\gamma_o} \frac{\sin\omega_B t}{\frac{1}{2} - n_s}, \qquad (56)$$

where

$$\omega_B = \frac{\Omega_{oz}}{\gamma_o} \frac{B_z}{B_\theta} (1/2 - n_s).$$

According to Eq. (55), when $n_s \ll 1$, i.e., for low current beams, thermal effects increase substantially the minor radius of the beam. In such beams the minor radius varies as $2r_o \Delta\gamma/\gamma_o$.

In contrast, when $n_s \gg 1$, i.e., for high current beams, thermal effects do not change significantly the minor radius of the beam, which varies as $(\frac{r_o}{n_s}) \frac{\Delta\gamma}{\gamma_o}$.

The effect of the axial energy spread on the minor cross-section of the beam in a modified betatron geometry has been studied numerically. Results from both the high and low current beams are given in Fig. 18. In these two runs the various parameters have the values listed in Table III. In the high current beam case the minor radius expands by approximately a factor of two. However, in the low current

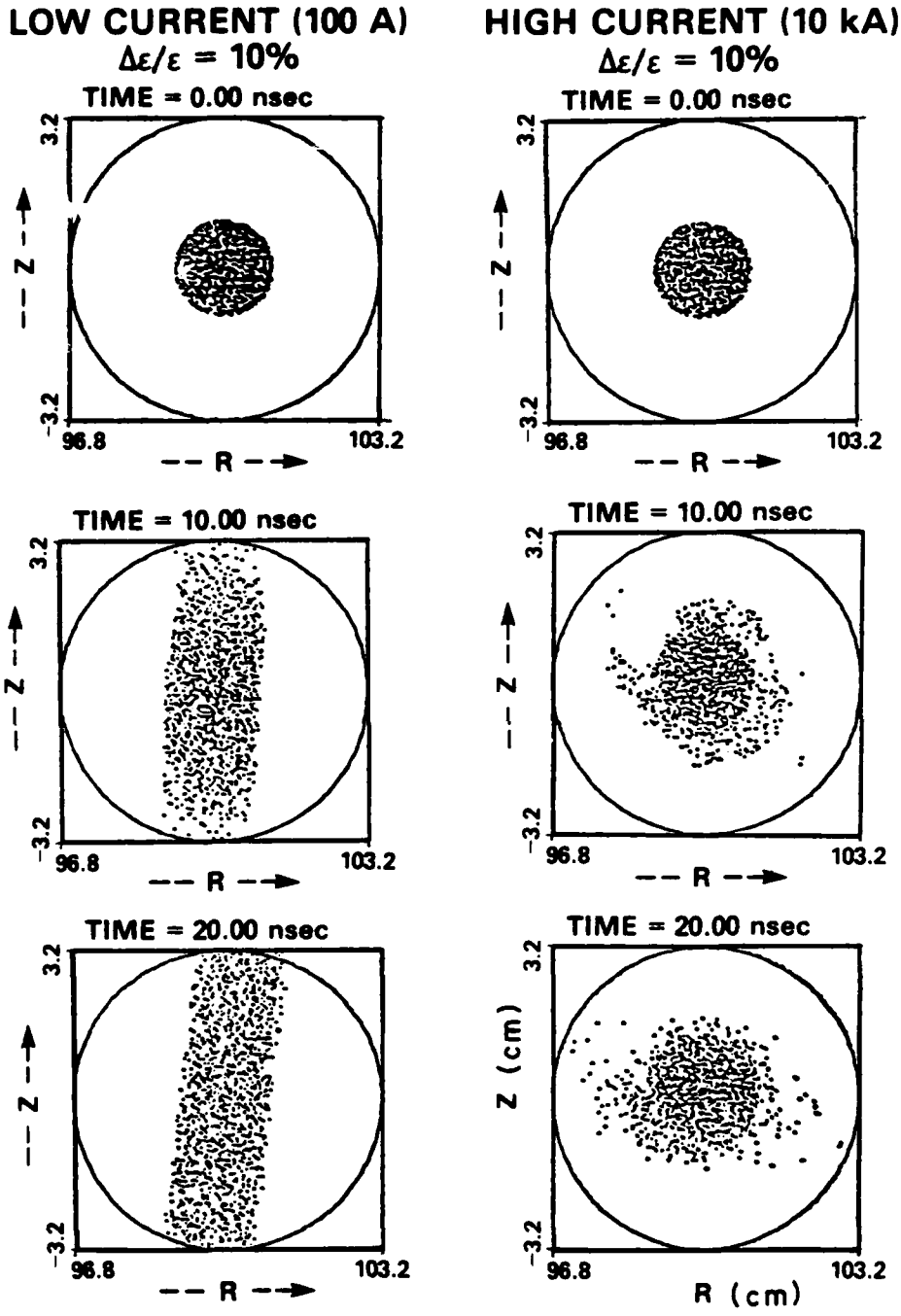

Figure 18. Snap-shots of the electron ring minor cross-section for low and high current. The values of the various parameters for this run are listed in Table II. The energy spread in both cases is 10%.

Table III.

Parameters	Low Current	High Current
Beam Current (kA)	0.1	10
Beam Energy (MeV)	3	3
Energy Spread (%)	10	10
Major Radius (cm)	100	100
Beam Minor Radius (cm)	1	1
Initial Betatron Field (G)	116	146
Toroidal Field (kG)	1.4	1.4
External Field Index	0.5	0.35
Self Field Index (n_s)	0.37	23.4
Torus Minor Radius (cm)	3.2	3.2

beam run the beam expands significantly and strikes the wall. Therefore, a substantial energy spread can be tolerated in high current beams without a catastrophic expansion of the minor radius of the beam. Such energy spread may be required to stabilize the various disruptive instabilities.[16-18]

VII. Summary

In this paper we review the dynamics of ultra-high current electron rings in the modified betatron configuration. Our discussion addresses mainly the evolution of the electron ring after injection. The formation of the ring during injection has been analyzed and reported previously.[19]

Our work includes both analytical and numerical results for "cold" and "hot" rings. The conclusion of these studies is that equilibrium states of ultra-high current rings in a modified betatron exist over a wide range of parameters. These equilibria are realistic and accessible with state of the art injectors.

The results presented in this paper are based on several simplified assumptions. Among them, we have assumed that the various fields are free of errors, the conducting wall that surrounds the electron ring was assumed to be smooth, i.e., without ports and gaps and the external field index was assumed to be constant in time and space. The consequences of these assumptions is presently under investigation.

Acknowledgments

The authors are greatful to Prof. D. Kerst as well as to the members of the Special Focus "Advanced Accelerator" and in particular to Drs. J. Golden, J. Pasour and F. Mako for many illuminating discussions.

Appendix A

Diffusion of the self magnetic field of the beam through a conducting liner.

The purpose of this appendix is to briefly outline the calculation of the diffusion of the self magnetic field of the beam through a conducting liner. To simplify the analysis, it is assumed that the electron beam is located along the axis of a straight, circular cylinder of inner radius a, outer radius b and thickness $\delta = b-a$, as shown in Fig. 9. In addition, it is assumed that the current of the electron beam is a step function that is turned-on at t=0. Since the problem of interest is that of an electron ring inside a torus, it is further assumed that the axial inductive electric field goes to zero at $r=r_0$, where r_0 is the major radius of the torus.

Neglecting the displacement current (quasi-static approximation), the fields inside the cylindrical conducting shell ($a \leq r \leq b$) are given in MKS units by

$$\nabla \times \vec{H} = \vec{J}, \qquad \text{(A-1)}$$

$$\nabla \cdot \vec{B} = 0, \qquad \text{(A-2)}$$

$$\nabla \times \vec{E} = -\frac{\partial \vec{B}}{\partial t}, \qquad \text{(A-3)}$$

and

$$\vec{J} = \sigma \vec{E}, \qquad \text{(A-4)}$$

where $\vec{J}$ is the current density, $\vec{H}$ is the magnetic field, $\vec{B}$ is the magnetic induction and σ the conductivity of the conductor.

Assuming that all quantities are independent of z and ϕ, Eqs. (A-1) to (A-4) can be combined to give a diffusion equation for the azimuthal component of the magnetic field

$$\frac{\partial}{\partial r}\left[\frac{1}{r}\frac{\partial}{\partial r}\left(r\,H_{\phi}(r,t)\right)\right] = \sigma\mu\frac{\partial H_{\phi}}{\partial t}(r,t)\,. \qquad \text{(A-5)}$$

For $r < a$ and $r > b$, the conductivity is equal to zero and Eq. (A-5) becomes

$$\frac{\partial}{\partial r}\left[\frac{1}{r}\frac{\partial}{\partial r}\left(r\,H_{\phi}(r,t)\right)\right] = 0\,, \qquad \text{(A-6)}$$

with the only acceptable solutions

$$H_{\phi}(r,t) = \frac{I}{2\pi r}\,\Theta(t),\ r_b \leq r \leq a \qquad \text{(A-7)}$$

$$H_{\phi}(r,t) = H_{\phi}(b,t)\ b/r,\ r \geq b \qquad \text{(A-8)}$$

where $\Theta(t)$ is the step function, and r_b is the beam radius.

To complete the specification of the problem we have to introduce boundary conditions. From Eqs. (A-3) and (A-8), we get

$$\frac{\partial E_z}{\partial r} = \mu\frac{\partial H_{\phi}(b,t)}{\partial t}\,\frac{b}{r}\,,$$

which after integration yields

$$E_z(r,t) = \mu\frac{\partial H_{\phi}(b,t)}{\partial t}\,b\,\ell n\,\frac{r}{r_o}\,, \qquad \text{(A-9)}$$

where we have assumed that $E_z(r,t)$ is zero at $r=r_0$.

Combining Eqs. (A-1), (A-4) and (A-9) at r=b, we obtain the first boundary condition, namely

$$\left[\frac{1}{r}\,\frac{\partial}{\partial r}\left(rH_{\phi}\right)\right]_{r=b} = \mu\frac{\partial H_{\phi}}{\partial t}(b,t)\ b\ \ell n\,\frac{b}{r_0}. \qquad \text{(A-10)}$$

The second boundary condition is furnished from the continuity of the magnetic field at r = a, i.e.,

$$\frac{I}{2\pi a}\,\Theta(t) = H_\phi(a,t). \qquad \text{(A-11)}$$

Since the magnetic field is zero at t=0, Eqs. (A-5), (A-9) and (A-10) take the following forms in their transformed state

$$\frac{\partial^2 \hat{H}_\phi}{\partial r^2} + \frac{1}{r}\,\frac{\partial \hat{H}_\phi}{\partial r} - \left(\frac{1}{r^2} + \sigma\mu p\right)\hat{H}_\phi = 0, \qquad \text{(A-12)}$$

$$\left[\frac{\partial}{\partial r}\left(r\hat{H}_\phi\right)\right]_{r=b} = \sigma\mu p\hat{H}_\phi(b,t)\; b^2 \ell n\,\frac{b}{r_0}, \qquad \text{(A-13)}$$

and

$$\frac{I}{2\pi a p} = \left[\hat{H}_\phi\,(r,t)\right]_{r=a}, \qquad \text{(A-14)}$$

where, the Laplace transform of H_ϕ is defined by

$$\hat{H}_\phi\,(r,p) = \int_0^\infty e^{-pt} H_\phi\,(r,t)\,dt, \qquad \text{Re}\,(p) > \tau.$$

Equation (A-12) is the modified Bessel equation and its solution is

$$\hat{H}_\phi\,(r,p) = AI_1(\lambda r) + BK_1(\lambda r),$$

where A and B are constants and $\lambda^2 = \sigma\mu p$.

The two constant coefficients A and B are determined from Eqs. (A-13) and (A-14) and are:

$$A = \left(\frac{I}{2\pi a p \Delta} \right) \left[K_0(\lambda b) + \lambda b \ \ell n \frac{b}{r_0} K_1(\lambda b) \right] ,$$

$$B = \left(\frac{I}{2\pi a p \Delta} \right) \left[I_0(\lambda b) - \lambda b \ \ell n \frac{b}{r_0} I_1(\lambda b) \right] ,$$

where

$$\Delta = K_0(\lambda b) \ I_1(\lambda a) + I_o(\lambda b) K_1(\lambda_a) + \lambda b \ell n \frac{b}{r_0} \left[K_1(\lambda b) \ I_1(\lambda a) \right.$$

$$\left. - K_1(\lambda b) \ I_1(\lambda b) \right]. \qquad \text{(A-15)}$$

The magnetic field in the region $a \leq r \leq b$ as a function of space and time can be obtained by inverting the Laplace transform, i.e.,

$$H_\phi(r,t) = \frac{I}{2\pi i} \int_{c-i\infty}^{c+i\infty} dp \frac{e^{pt}}{2\pi a p \Delta} \left\{ \left[K_0(\lambda b) + \lambda b \ \ell n \ \frac{b}{r_0} K_1(\lambda b) \right] I_1(\lambda r) \right.$$

$$\left. + \left[I_0(\lambda b) - \lambda b \ \ell n \ \frac{b}{r_0} I_1(\lambda b) \right] K_1(\lambda r) \right\} , \qquad \text{(A-16)}$$

where the path of integration is a vertical line in the complex p-plane to the right of all singularities of the integrand.

Equation (A-16) has a simple pole at p=0 of residue a/r and an infinite set of simple poles at Δ=0.

Contour integration of Eq. (A-16) gives

$$H_\phi(r,t) = \frac{I}{2\pi a} \left\{ \frac{a}{r} + \sum_{s=1}^{\infty} e^{-\alpha_s^2 t/\sigma\mu_0} \left[Y_0(\alpha_s b) J_1(\alpha_s r) - Y_1(\alpha_s r) \ J_0(\alpha_s b) \right.\right.$$

$$\left.\left. + \alpha_s b \ \ell n \frac{b}{r_0} \left[Y_1(\alpha_s b) J_1(\alpha_s r) - Y_1(\alpha_s r) \ J_1(\alpha_s b) \right] \right] \Big/ \alpha_s \left(\frac{dD}{d\alpha} \right)_{\alpha=\alpha_s} \right\} \qquad \text{(A-17)}$$

where $\mu = \mu_0$, $\lambda = i\alpha$, Y,J are the Bessel functions, α_s are the roots of equation

$$Y_0(\alpha_s b)J_1(\alpha_s a) - Y_1(\alpha_s a)J_0(\alpha_s b) + \alpha_s b \ln \frac{b}{r_0} [Y_1(\alpha_s b)J_1(\alpha_s a) - Y_1(\alpha_s a)J_1(\alpha_s b)] = 0, \quad \text{(A-18)}$$

and

$$\alpha_s \left(\frac{dD}{d\alpha}\right)_{\alpha=\alpha_s} = \alpha_s a [Y_0(\alpha_s b)J_0(\alpha_s a) - Y_0(\alpha_s a)J_0(\alpha_s b)] - \alpha_s b[Y_1(\alpha_s b)J_1(\alpha_s a) - Y_1(\alpha_s a)J_1(\alpha_s b)] + \alpha_s b \ln \frac{b}{r_0} \{b\alpha_s [Y_0(\alpha_s b)J_1(\alpha_s a) - Y_1(\alpha_s a)J_0(\alpha_s b)] + \alpha_s a [J_0(\alpha_s a)Y_1(\alpha_s b) - Y_0(\alpha_s a)J_1(\alpha_s b)]\}.$$

For $\alpha_s a \gg 1$, Eq. (A-17) is reduced to

$$H_\phi(r,t) \approx \frac{I}{2\pi a} \left\{ \frac{a}{r} \sqrt{\frac{a}{r}} \sum_{s=1}^{\infty} e^{-\alpha^2 t/\sigma\mu_0} [\cos \alpha_s(b-r) + \alpha_s b \ln \frac{b}{r_0} \sin \alpha_s(b-r)] \Big/ \left(\alpha_s \delta \sin(\alpha_s \delta) - \alpha_s^2 b \ln \frac{b}{r_o} \cos \alpha_s \delta\right)\right\}, \quad \text{(A-19)}$$

where α_s are now the roots of

$$\cos(\alpha_s \delta) + \alpha_s b \ln \frac{b}{r_o} \sin(\alpha_s \delta) = 0. \quad \text{(A-20)}$$

Equations (A-19) and (A-20) can be further simplified when $\alpha_s \delta \ll 1$. In this case

$$H_\phi(r,t) = \frac{I}{2\pi a}\left\{\frac{a}{r} - \left(\frac{a}{r}\right)^{1/2}\left[\cos\alpha_s(b-r) + \alpha_s b \ln\frac{b}{r_0}\sin\alpha_s(b-r)\right]\right.$$

$$\left. e^{-\alpha_s^2 t/\sigma\mu_0}\right\},$$

which at r=b, becomes

$$H_\phi(b,t) = \frac{I}{2\pi b}\left\{1 - e^{-\alpha_s^2 t/\sigma\mu_0}\right\},$$

where

$$\alpha_s^2 = \frac{1}{\delta b \ln\frac{r_0}{b}}. \qquad \text{(A-21)}$$

Therfore, to lowest order, the magnetic field in the region $r \geq b$ is

$$H_\phi(r,t) = \frac{I}{2\pi r}\left\{1 - e^{-\alpha_s^2 t/\sigma\mu_0}\right\}, \quad r \geq b, \quad \text{MKS} \quad \text{(A-22)}$$

or

$$H_\phi(r,t) = \frac{2I}{rc}\left\{1 - e^{-\alpha_s^2 tc^2/4\pi\sigma}\right\}. \quad \text{CGS} \quad \text{(A-23)}$$

Under the same approximations, the electric field at the inner edge (r=a) of the conducting shell is

$$E_z(a,t) = -\frac{I}{2\pi\sigma}\alpha_s^2 \ln\left(\frac{r_0}{b}\right) e^{-\alpha_s^2 t/\sigma\mu_0}, \qquad \text{MKS} \quad \text{(A-24)}$$

or

$$E_z(a,t) = -\frac{I}{2\pi\sigma}\alpha_s^2 \ln\left(\frac{r_0}{b}\right) e^{-\alpha_s^2 tc^2/4\pi\sigma}. \qquad \text{CGS}$$

Since the electric field is uniform in the region $r \leq a$, Eq. (A-24) gives also the electric field that acts on the beam. Substituting Eq. (A-24) into the energy rate equation

$$mc^2 \frac{d\gamma}{dt} = -e\vec{v} \cdot \vec{E},$$

we obtain for highly relativistic beams

$$\frac{\Delta\gamma}{\gamma} \approx -2 \frac{\nu}{\gamma} \ln \frac{r_0}{b} . \qquad \text{A-25)}$$

For $\frac{r_0}{b} = 10$ and $\frac{\nu}{\gamma} = 0.1$, Eq. (A-25) gives $\frac{\Delta\gamma}{\gamma} = 0.46$, i.e., a substantial reduction in the energy of the beam. However, for highly relativistic beams $v_z \simeq c$ and thus the current of the beam remains approximately constant.

Appendix B

Description of the Particle in Cell Computer Code

The NRL modified betatron accelerator is designed for a maximum $v/\gamma_o \approx 0.1$, i.e., the current is high enough so that the self-fields of the ring can exceed the externally applied fields. A realistic theoretical description must therefore self-consistently include the beam's self fields as well as the effect of surrounding walls. Since this is difficult analytically, particularly if the ring is displaced substantially from the center of the minor cross-section of the torus, numerical simulations are useful both in gaining insight into the important physical processes as well as to provide a method to check the applicability of specific assumptions in an analytic model.

The dynamics of the accelerated electron ring are determined by forces that vary on a number of different time scales which range from the electron cyclotron period, i.e., a few nanoseconds to the beam acceleration time, which is of order a millisecond. The code described here is taylored to simulate efficiently the various phenomena on the intermediate time scale. This time scale is characteristic of the drift (bounce) motion of the ring after equilibrium has been established, rather than the rapid evolution occuring at injection. Simulation of a single turn around the major axis that lasts about 20 nsec using 4K particles on a 64 x 64 grid and typically takes about one minute on the NRL Texas Instruments ASC.

The simulation code is r-z, spatially two dimensional, i.e. $\frac{\partial}{\partial\theta} = 0$, but with three velocity components. Although B_θ is used in calculating the particle trajectories, it is not solved self-consistently, i.e., is assumed to be generated from external coils only. This assumption is valid to first order in v/γ. The radiative term (displacement current) is also ignored, i.e., the code uses the

Darwin model for Maxwell's equations.

The electrostatic potential is computed from Poisson's equation

$$\nabla^2 \Phi = \rho/\varepsilon_o, \tag{B-1}$$

and the magnetic vector potential from

$$\nabla^2 A_\theta - \frac{A_\theta}{r^2} = -\mu_o J_\theta, \tag{B-2}$$

with the boundary condition $\Phi = A_\theta = 0$ at the conducting wall.

Equations (B-1) and (B-2) are solved by Fourier decomposition in the z-direction and then by Gaussian elimination of the resultant tridiagonal matrix of equations obtained from a 3-point differencing scheme for ∇_r^2. The inverse Fourier transform yields A_θ and Φ on the grid. Note that the θ particle velocities are advanced using the conservation of cannonical momentum in the θ direction, the equation for A_θ is therefore not properly time centered since the velocities from the previous time step are used to calculate the currents from the cannonical momenta. This method was chosen primarily for its speed and simplicity but care must be taken in applying the code when the inductive acceleration of particles in the θ direction is significant.

If boundary conditions other than A_θ or Φ equal zero on a rectraqular grid are desired, it is possible to obtain relatively arbitrary boundary conditions using the capacitive matrix(Buneman) technique. In this method a matrix is generated which is the Green's function for discrete "wall" points within the system. Then at each time step the field solver described above is used. The potential at the discrete (wall) points is obtained. By multiplying this vector potential by the invense matrix obtained previously a set of (wall) currents or changes is generated, which

is used to specify the wall potential. These "wall" sources are then added to the original beam source and the field solver is used again. The result by the principle of superposition is correct inside the system and has the correct boundary condition on the "wall".

Particle Push

The motion of the electrons is governed by the Lorentz force

$$\frac{d(\gamma\vec{V})}{dt} = \frac{q}{m_0}\left(\vec{E} + \vec{V} \times B\right),$$

where $\vec{E}$ and $\vec{B}$ are the total electric and magnetic field respectively.

In component form the equations used to update the velocities and positions at each time step are

$$\gamma V_\theta = \frac{P_\theta}{m_o r} - \frac{q}{m_o} A_\theta \tag{B-3}$$

$$\frac{d(\gamma V_r)}{dt} = \frac{q}{m_o}\left(E_r + V_\theta \times B_z - V_z \times B_\theta\right) + \frac{\gamma V_\theta^2}{r} \tag{B-4}$$

$$\frac{d(\gamma V_z)}{dt} = \frac{q}{m_o}\left(E_r - v_\theta \times B_z + V_z \times B_\theta\right) \tag{B-5}$$

$$\frac{dr}{dt} = V_r \tag{B-6}$$

$$\frac{dz}{dt} = V_z \tag{B-7}$$

Equation (B-3) is used at each timestep to compute γV_θ. Equations (B-4) and (B-5) are coupled. To advance these velocities a leap-frog scheme is employed. At time t all fields, positions and V_θ are known exactly. V_r and V_z however are known at t+1 and the velocities will be advanced to t+1/2. Before the equations are

differenced, it is convenient to rewrite the equations in terms of the relativistic momenta. Letting

$$\vec{U} = \gamma\vec{V}$$

the equations (B-3), (B-4) and (B-5) can be written as

$$U_\theta = \frac{P_\theta}{m_o r} - \frac{q}{m_o} A_\theta \qquad \text{(B-3a)}$$

$$\frac{dU_r}{dt} = \frac{q}{\gamma m_o} (\gamma E_r + U_\theta x\ B_z - U_z x\ B_\theta) + \frac{U_\theta^2}{\gamma r} \qquad \text{(B-4a)}$$

$$\frac{dU_z}{dt} = \frac{q}{\gamma m0} (\gamma E_z - U_\theta x\ B_r + U_r x\ B_\theta) \qquad \text{(B-5a)}$$

$$\frac{dr}{dt} = \frac{U_r}{\gamma} \qquad \text{(B-6a)}$$

$$\frac{dz}{dt} = \frac{U_z}{\gamma} \qquad \text{(B-7a)}$$

This formulation is then differenced by substituting

$$\frac{\vec{U}^{+\,1/2} - \vec{U}^{t-1/2}}{\Delta t} \qquad \text{for} \qquad \frac{d\vec{U}}{dt}$$

and

$$\frac{\vec{U}^{t+1/2} + \vec{U}^{t-1/2}}{2} \qquad \text{for} \qquad \vec{U}\ .$$

After making these substitutions in equations (B-4a) and (B-5a) it is straightforward, if somewhat tedious, to solve the two coupled equations for $U_z^{t+1/2}$ and

$U_r^{t+1/2}$. Since U_r and U_z are calculated at the half-timesteps while U_θ is known at the full timesteps, γ is not known at time t. This difficulty is overcome using iteration.

After advancing the velocities the particle positions are advanced using a simple centered difference

$$r^{t+1} = r^t + \delta T. \frac{U_r}{\gamma} ,$$

and

$$z^{t+1} = z^t + \delta T. \frac{U_z}{\gamma} .$$

Once all the velocities and positions are found the new current and charge densities are used to update the fields and a new time step begins.

References

1. T. J. Fessenden et. al; Proc. of the Intern. Top. Conf. on High-Power Electron and Ion Beam Research and Technology; Palaiseau, France, June 29 - July 3, 1981 p. 813.
2. R. Briggs, Proc. 1981 Particle Accel. Conf. to be published in IEEE Trans. Nucl. Sci. NS-28 (June 1981).
3. A. I. Paulovskii et. al; Sov. Phys. Tech. Phys. 22, 218 (1977).
4. P. Sprangle and C. A. Kapetanakos, J. Appl. Phys. 49, 1 (1978).
5. P. Sprangle, C. A. Kapetanakos and S. J. Marsh; Proc. of the Intern. Top. Conf. on High-Power Electron and Ion Beam Research and Technology; Palaiseau, France, June 29 - July 3, 1981 p. 803; Also NRL memo Report No. 4666 (1981).
6. G. Barak, D. Chernin, A. Fisher, H. Ishizuka and N. Rostoker; Proc. of the Intern. Top. Conf. on High Power Electron and Ion Beam Research and Technology; Palaiseau, France, June 29 - July 3, 1981, p. 795.
7. H. S. Uhm and R. C. Davidson, UIT, Plasma Fusion Center Report No. JA-81-30 (1981).
8. D. W. Kerst et. al. Rev. Sci. Inst. 21, 462 (1950).
9. D. W. Kerst, Nature, 157, 90 (1940).
10. R. C. Davidson, Theory of Nonneutral Plasmas, W. A. Benjamin, Inc. 1974.
11. D. P. Chernin and P. Sprangle, Particle Accelerators 12, 85 (1982).
12. G. Schmidt, Phys. Rev. Lett. 26, 952 (1971).
13. J. D. Lawson, The Physics of Charged Particle Beams; Clarendon Press - Oxford, 1977.
14. P. Sprangle and C. A. Kapetanakos, NRL memo report No. (1982).
15. V. K. Neil, Jason, Tech. Report JSR-79-10 (1979).

16. P. Sprangle and J. Vomvoridis, NRL memo report no. 4688.

17. D. P. Chernin and P. Sprangle, Particle Accelerators, 12, 101 (1982).

18. T.P. Hughes and B.B. Godfrey, Mission Research Corp. Report No. AMRC-R-354, 1982; also AMRC-R-322, 1982.

19. C. A. Kapetanakos, P. Sprangle and S. J. Marsh, NRL Memo Report No. 4835, 1982; Phys. Rev. Letts. 49, 741 (1982).